TECHNISCHE UNIVERSITÄT WIEN
Vienna University of Technology

Universität für Bodenkultur Wien
University of Natural Resources and Life Sciences, Vienna

MASTER'S THESIS

BIOLOGICAL ACTIVITY OF CURCUMIN-LOADED CYCLODEXTRIN-DECORATED SUPERPARAMAGNETIC IRON OXIDE NANOPARTICLES

AKOS MIHALY

SUPERVISORS
DR. ANTONINO PUGLISI
UNIV.-PROF. DR. ERIK REIMHULT
UNIV.-PROF. DR. PETER ERTL

INSTITUTE OF BIOLOGICALLY INSPIRED MATERIALS
DEPARTMENT OF NANOBIOTECHNOLOGY
UNIVERSITY OF NATURAL RESOURCES AND LIFE SCIENCES

VIENNA
AUSTRIA

2022

TABLE OF CONTENTS

ABSTRACT

Curcumin, a curcuminoid from *Curcuma longa*, possesses enormous potential as a therapeutic agent in numerous applications, including antibacterial and anticancer therapy. However, its low water solubility and poor bioavailability severely hamper its use as a therapeutic agent. To overcome such limitations, drug delivery systems (DDS) are being investigated in order to improve their pharmacokinetic profile.

In this context, nanoparticles have been actively studied as promising DDS as they possess a number of desirable characteristics to improve drug delivery, including a large surface area-to-volume ratio, that enables better drug uptake and controlled drug release kinetics.

Cyclodextrins are a family of naturally occurring cyclic oligosaccharides derived from the enzymatic conversion of starch. They have been employed in the pharmaceutical industry in recent years. Cyclodextrins are water-soluble and possess an interior hydrophobic cavity that can form inclusion complexes with a variety of different guest molecules, including curcumin. However, the administration of cyclodextrin in its monomeric form suffers from several drawbacks due to its faster clearance. Nanoparticle packaging of cyclodextrin might help overcome some of its limitations and improve bioavailability. Such nanoparticles could also be used for multi-functional therapeutics by delivering different types of hydrophobic cargo and removing unwanted hydrophobic constituents, such as cholesterol, a useful therapy in neurodegenerative disease treatment.

In this work, we introduce different delivery options for curcumin using β-cyclodextrins and cyclodextrin-appended superparamagnetic iron oxide nanoparticles. We also aim to identify the ability of β-cyclodextrin to sequester cholesterol and reduce bacterial growth. We report the cholesterol-mopping activity of cyclodextrin-decorated superparamagnetic iron oxide nanoparticles in cholesterol-impaired CHO cell lines. Moreover, apoptotic properties on HepG2 cells are assessed for free curcumin and curcumin-loaded on either cyclodextrin or cyclodextrin-functionalized superparamagnetic iron oxide nanoparticles. Finally, we investigate free curcumin, free cyclodextrin, and curcumin-loaded cyclodextrins for their antibacterial effect on *Staphylococcus aureus*.

Keywords: curcumin, β-cyclodextrin, inclusion complex, SPIONs, drug delivery, cholesterol-mopping, internalization, apoptosis, antibacterial activity

ABBREVIATIONS

CD	Cyclodextrin
β-CD	β-cyclodextrin
CUR	Curcumin
CUR-CD	Curcumin-β-cyclodextrin inclusion complex
SPION	Superparamagnetic iron oxide nanoparticle
CySPION	Cyclodextrin-decorated superparamagnetic iron oxide nanoparticles
CUR-CySPION	Curcumin-loaded cyclodextrin-decorated superparamagnetic iron oxide nanoparticles
NP	Nanoparticle
CHO	Chinese Hamster Ovary cells
NPC	Niemann Pick type C
DMSO	Dimethyl sulfoxide
HPβCD	2-hydroxypropyl-β-cyclodextrin
DMEM	Dulbecco's Modified Eagle Medium
PenStrep	Penicillin-Streptomycin solution
HEPES	4-(2-hydroxyethyl)-1-piperazineethanesulfonic acid
FCS	Fetal calf serum
MEM	Minimum Essential Medium Eagle
PBS	Phosphate-buffered saline
TSB	Tryptic soy broth

MOTIVATION AND AIMS

Curcumin has been reported to have diverse pharmacological activities. However, its clinical efficacy is limited by its low aqueous solubility and stability, leading to poor bioavailability. It is necessary to develop new strategies to improve the effectiveness of curcumin delivery.

β-cyclodextrin is a suitable carrier that can enhance solubility, stability, and bioavailability of small hydrophobic molecules such as curcumin by forming an inclusion complex with the compound. There is also an increased interest in cyclodextrins as medicinal agents based on their property of extracting cell membrane cholesterol and providing a suitable carrier system for drug delivery. However, cyclodextrins also suffer from fast clearance and poor bioavailability in parts of the body, which are related to both biochemical properties and size. Packaging of cyclodextrins into nanoparticles could remedy these weaknesses and thereby improve drug delivery of curcumin via its β-cyclodextrin inclusion complex. Superparamagnetic iron oxide nanoparticles (SPIONs) have been widely used in targeted drug delivery. Studies have shown that SPIONs are physiologically well-tolerated, and they can be surface coated with different ligands to prevent their rapid clearance from circulation.

We aimed to improve the efficacy of curcumin in cancer and antibiotic therapies by formulating curcumin as a β-cyclodextrin inclusion complex grafted on core-shell poly(methyloxazoline)-grafted SPION, called CUR-CySPION. This theranostic agent could combine imaging, drug formulation, and triggered drug delivery. We accomplished our aim by a stepwise assembly of the therapeutic agent, detailed physicochemical characterization, and comparing different formulations on *in vitro* cell and bacteria cultures.

INTRODUCTION

1.1 History of nanotechnology

Richard Feynman's lecture in 1959 entitled "*There's Plenty of Room at the Bottom: An Invitation to Enter a New Field of Physics*" opened a new era in technology, which has become the field of nanotechnology, one of today's most dynamically developing field of science and technology [1]. It deals with the production, characterization, and usage of different nanostructures. In principle, nanomaterials are described as having at least one dimension less than 100 nm. They have gained prominence in technological advancements because, in this size range, materials have different, enhanced properties over their bulk counterparts. These new properties often emerge from the increased surface-to-volume ratio. This implies that size can influence the physio-chemical properties of the substances, e.g., density, crystal structure, melting point, wettability, catalytic activity, magnetic-and optical properties, light absorption and scattering, electrical-and thermal conductivity [2].

Humans already exploited nanoparticles thousands of years ago, unknowingly. The Ancient Egyptians used nanomaterials based on a synthetic chemical process to synthesize lead(II) sulfide nanoparticles for hair dye [3]. Mayan blue, the dye used by the ancient Maya, is a composite of organic and inorganic materials [4]. Damascus steel swords have become legendary for their strength and flexibility. It was since they contained carbon nanotubes [5]. Depending on their site, gold and silver nanoparticles make the painted window glass red, orange, purple, green and blue. The Lycurgus cup in the British Museum emits green light when it is lit from the outside but red when it is lit from the inside. These colors are due to the encapsulated silver and gold nanoparticles, as they scatter light differently in different directions. The red color is due to gold nanoparticles [6].

1.2 Types of nanomaterials

Nanomaterials can be classified into different groups upon their origin. Naturally produced nanomaterials can be found in the bodies of organisms, plants, animals and humans. Incidental nanomaterials are produced as an unintentional byproduct of industrial processes, such as nanoparticles from vehicle engine exhaust or welding fumes. Engineered nanomaterials are manufactured by humans to have certain required properties for desired applications.

Volcanic eruptions and forest fires and dust storms are reported to produce a significant amount of nanoparticle matter that affects worldwide air quality [7]. Dust storms can migrate the nano-sized minerals and anthropogenic pollutants to thousands of kilometers away. Asthma is an outstanding health issue that is caused by terrestrial airborne dust particles. Dust nanoparticles containing metals have the capability of damaging lung tissues by producing reactive oxygen species [8]. Volcanic eruptions lead to the propulsion of a tremendous number of aerosols and fine particles into the atmosphere. These volcanic particles may contain heavy metals that are toxic to humans. The short-term effects of such particles include skin, throat, nose and eye irritations, while the long-term effects could be more serious, such as podocinids and Kaposi's sarcoma. Podociniosis leads to localized fluid retention in the lower limbs [8]; Kaposi's sarcoma affects the blood and lymph vessels [9].

Naturally occurring nanomaterials are continuously being formed and distributed throughout ground and surface water, the oceans, continental soil, and the atmosphere. Nanoparticles and nanostructures are also present in living beings, from microorganisms, such as bacteria, algae to viruses, and complex organisms, such as plants, insects, birds, animals and humans. Recent developments of imaging and other analytical techniques have improved our ability to identify the morphology of these nanomaterials, which leads to a better understanding of their complex functions in living systems. Knowledge about the nanostructures present in microorganisms is crucial for their further usage in biomedical applications [10]. As an example, magnetotactic bacteria are very useful in producing magnetic iron oxide nanoparticles that possess the unique property of being ferrimagnetic. Hence, biocompatible magnetic nanoparticles could be synthesized using magnetotactic bacteria [11] that help in targeted cancer treatment via magnetic hyperthermia and magnetic resonance imaging (MRI). The bacterial magnetic particles which are produced by the bacterium are proposed to perform as a compass-like bio-needle that helps the bacteria to migrate under the impact of the Earth's geomagnetic field [12].

A well-known property of lotus leaves is superhydrophobicity, which makes their leaves excellent model surfaces having a self-cleaning effect. Self-cleaning plant leaves are found to have a defined micro- or nano-scale topography, prohibiting water droplets to spread and instead form droplets that roll off and remove dirt with them. Mimicking the structure of superhydrophobic leaves is a great idea to develop self-cleaning surfaces. [13].

As for animals, many of them have the exceptional ability to attach themselves to ceilings or vertical walls despite gravity. This property, for instance, with geckos is linked to the nanometer-sized hair-like structures in their feet that are aligned in a series of small ridges.

This increases the surface area of their feet and leads to a van der Waals interaction mediated strong surface adhesion [14].

Simple combustion in vehicles, fuel oil, and coal for power generation [15], airplane engines, chemical manufacturing, welding, ore refining, and smelting are some of the anthropogenic activities that lead to nanoparticle formation [16]. It has been shown that carbon nanotubes and fibers are released as byproducts during diesel and gas combustion processes [17].

Smoking cigarettes and building demolition are additional anthropogenic actions that lead to the expansion of nanoparticles into the atmosphere. Cigarette smoke consists of many nano-sized chemical compounds ranging from 10 to 700 nm [18]. Cigarette smoke can lead to many diseases, including chronic respiratory illness, cardiovascular disease, lung cancer, and chronic middle ear disease [19]. When a building is demolished, debris, lead, glass, asbestos fibers and other toxic nano-sized particles are released [20].

Nanoparticles are often incorporated in biomedical and healthcare products. Nanoparticles, such as carbon [21], titanium oxide [22], hydroxyapatites [23] are in use in cosmetics, sporting goods, sunscreen and toothpaste. Gold nanoparticles are widely used in different applications, including wet wipes, sanitizer sprays, food storage containers, shampoos and toothpaste [24].

1.3 Nanoparticle corona

When nanoparticles are in a biological environment, they interact most strongly with proteins, which are abundant biomacromolecules in most biofluids, e.g., blood. Proteins can absorb onto the surface of nanoparticles, which is referred to as the formation of a *protein corona*. As the protein corona assembles, it determines the colloidal stability, interactions, and toxicity of NPs. Proteins strongly interacting with the surface define the so-called *hard corona*, while the external layer of loosely bound proteins is defined as the *soft corona* [25]. Regarding the relationship between the hard and soft corona, there were different theories claiming first the soft protein corona is being formed, which, over time, develops into a hard corona, while other research has suggested that hard and soft coronae are coexisting, core-shell-like formations [26].

It has been shown that not only proteins but other biomolecules (e.g., amino acids, carbohydrates, lipids and hormones) may be involved in the formation of the coronae, therefore it can be considered to be *biomolecular corona* as well [27]. The formation of a biomolecular

corona confers a kind of biological identity to the nanomaterials that enter the body, which appears in the form of specific interactions. These interactions determine the primary response of the organism to the nanoparticles. There have been plenty of studies on observing and understanding these interactions at the molecular level.

Nanoparticles have different chemical surface characteristics, which cause structural changes in the bound proteins. Certain physical properties, such as size, shape, curvature and surface, affect the structure of the bound proteins. Structural changes in corona proteins are biologically meaningful, as the corresponding loss of function may provoke the destruction of physiological homeostasis and unwanted immune response [28].

The formation of a protein corona is disadvantageous for most *in vivo* applications of nanoparticles. Corona proteins can eliminate the targeting ability of NPs, as the bound proteins may sterically mask the pre-coupled targeting ligands that recognize specific receptors or target molecules on cells. A surface protein ligand on the nanoparticle surface would lose its structure upon interacting with corona proteins. Interacting with cellular proteins, a nanoparticle protein corona could induce many signal modulations and toxic effects in cells. Different cellular responses occur, like inflammation, oxidative stress, DNA damage, apoptosis, etc.

It is clear that a surface modification of nanoparticles is necessary to prevent the uncontrolled formation of a protein corona. The surface modification must be properly designed to maintain a well-dispersed colloidal state and control the particles' protein interactions – and by this, achieve a reproducible specific function for clinical applications. Nanoparticle surface modifications can be performed in many ways and generally serve the purpose of controlling interactions with biomolecules in medical and biotechnological applications. Among the most important properties to control are hydration and surface charge. Polymers, such as poly(ethylene glycol) (PEG), poly(ethyl ethylene phosphate) (PEEP), and poly(2-methyl-2-oxazoline) (PMOXA) are widely used to create highly hydrated surfaces that sterically and osmotically resist protein adsorption [29]. Surface charge can significantly influence the conformation of bound proteins [30] and regulate protein adsorption, binding affinity, and structural changes.

It is important to mention that a good number of studies have suggested the use of the protein corona formation. Nanoparticles pre-incubated and pre-coated with proteins may gain a new biological identity. This might allow bypass the immunogenic response against nanoparticles by stealth effects, improvement targeting and stabilization against agglomeration [30].

1.4 Curcumin

Curcumin is the principal curcuminoid of the Indian spice turmeric. It is an orange-yellow hydrophobic polyphenol derived from the rhizome of the herb *Curcuma longa* (Figure 1). It has been widely studied for its range of biological activities in chronic diseases and has broad therapeutic efficacy. Curcumin has numerous pharmacological applications, including anticancer, antimicrobial, anti-inflammatory, antioxidant, and the treatment of cardiovascular and neurodegenerative diseases [31]. At the molecular level, curcumin has been shown to modulate multiple intracellular pathways associated with proliferation, survival, invasion, apoptosis and inflammation [32].

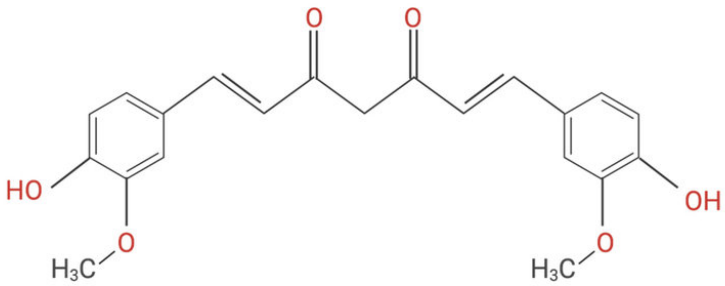

Figure 1. Chemical structure of curcumin

There are several mechanisms shown by which curcumin could have anti-cancer properties [33]. The anti-cancer properties of curcumin are associated with its ability to modulate the histone modulating enzymes connected to epigenetic pathways [34]. In studies conducted using PCM-3 prostate cancer cells *in vitro*, treatment with curcumin was shown to normalize the histone hyperacetylation associated with prostate cancer through the induction of p300 degradation [35]. Evidence suggests that curcumin has the capacity to inhibit DNA methylation, which also yields anti-cancer effects [32]. Cancer cells are known to have increased oxidative stress, which increases their vulnerability to damage by additional Reactive Oxygen Species (ROS) generation induced by exogenous agents. Curcumin was shown to stimulate ROS generation and apoptosis in PCa cells [36].

Despite the promising preliminary studies demonstrating the therapeutic promise of curcumin, it has not yet been approved as a treatment due to its low water solubility, rapid metabolism and poor bioavailability. In addition, it is sensitive to light, thermal treatment,

enzymes, oxygen and ascorbic acid [37]. On top of that, curcumin is highly unstable at the acidic pH of the gut and may be degraded before reaching the blood. Consequently, the optimum quantity of curcumin may not reach the blood, leading to no or little therapeutic effect [38]. Therefore, the search for an efficient and nontoxic carrier for curcumin is important. Formulating curcumin in a carrier system could help bypass some of the problems associated with the current administration of curcumin, such as cellular uptake and prolonged circulation.

The antibacterial effect of curcumin has been demonstrated against both Gram-positive and Gram-negative bacteria. It also inhibits bacterial biofilms, which are groups of cells embedded in a polymeric matrix tolerant to antimicrobial treatments. The antibacterial mechanism of action of curcumin involves the rupture of the cell membrane, interference with cellular processes by targeting DNA and proteins, and the inhibition of bacterial quorum sensing, which is a communication process mediated by the biochemical signal that regulates cell density and microbial behavior [39].

1.5 Cyclodextrin

Cyclodextrins (CDs) [40] are naturally occurring cyclic oligosaccharides derived from the enzymatic conversion of starch. They are composed of a varying number of glucopyranose units linked by α-(1,4)-glycosidic bonds that form a hollow cone-like toroid structure consisting of a hydrophobic cavity and a hydrophilic exterior (Figure 2). The number of glucopyranose units determines the cavity size and nomenclature of the CD, with the most common consisting of six, seven, or eight glucopyranose units and named α-, β- and γ-CD, respectively. This unique structure allows CDs to form water-soluble complexes with otherwise insoluble hydrophobic compounds docked in the internal cavity. This property of CDs has led to their application as delivery vehicles to improve the solubility, stability and bioavailability of many drugs via forming an inclusion complex [36].

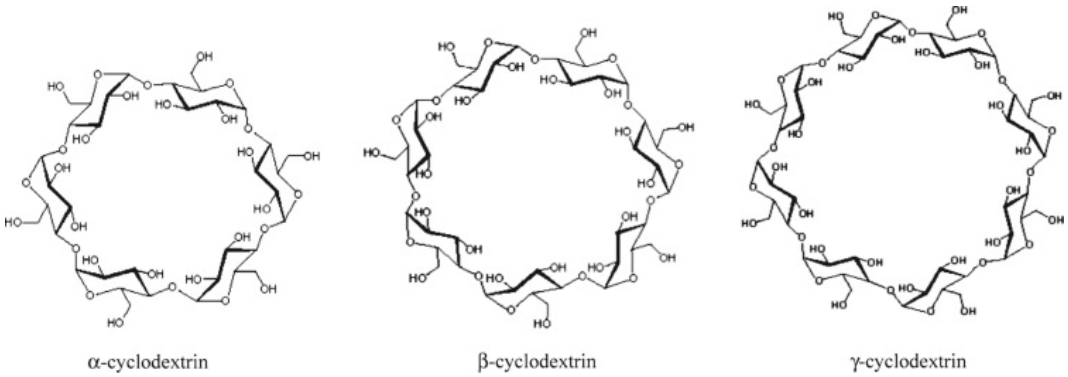

Figure 2. The chemical structure of cyclodextrins

The ability of the CDs to form inclusion complexes has two main advantages. Firstly, it increases the water solubility of hydrophobic compounds. The basic structure of CDs comprises a cyclic chain of carbohydrates oriented as the inner cavity is hydrophobic in character, while the outer surface is flanked by hydrophilic hydroxyl moieties. This allows hydrophobic molecules to be entrapped within the inner cavity of CDs while their outer surface permits aqueous solubility. Secondly, through the formation of the inclusion complex, the properties of the encapsulated compound are modified resulting in improved stability, bioavailability, oral administration and drug interaction with biological membranes or cells [41].

All three types of CDs can achieve inclusion complexes, although it is the relation of the size of their inner cavity to the complexed molecule which determines the success in complex formation. β-CDs have been the most suitable for hosting many biological compounds, such as vitamins, hormones [42], and other molecules, e.g., curcumin [37]. Curcumin forms inclusion complexes with β-cyclodextrin, in which a CD encapsulates one of the two of its phenyl rings (Figure 3), with the highest affinity for a complex with a β-CD dimer.

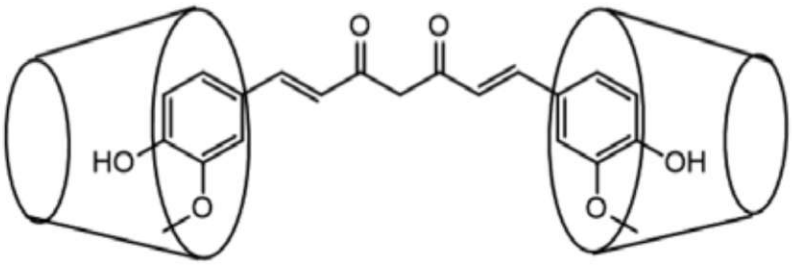

Figure 3. Schematic representation of the inclusion complex

1.5.1 Cyclodextrin applications

Cyclodextrins have recently been suggested as therapeutic agents in cholesterol-impaired diseases. Cholesterol plays an essential role in nearly all aspects of cellular structures and functions. It is a major component of cell membranes and serves as a precursor or cofactor for steroid hormone synthesis and other signaling molecules. Therefore, it has a critical role in body metabolism.

Membrane cholesterol must be maintained at a constant level. The homeostasis is maintained via a feedback mechanism that senses the level of cholesterol in the cells by membrane-bound transcription factors, known as sterol regulatory element-binding proteins (SREBPs), which modulate the transcription of genes encoding enzymes of cholesterol synthesis and uptake from plasma lipoproteins [43].

In principle, the reason cells release cholesterol could be that they produce a surplus to provide other cells, or they get rid of excess amounts to prevent sterol-induced damage. Depending on the purpose, cholesterol release is achieved by two pathways that involve certain lipid carriers - lipoproteins. The supply of cells with cholesterol is mediated by low-density lipoproteins (LDL) particles. The elimination of excess cholesterol happens in the liver and is mediated by high-density lipoprotein (HDL) particles [44].

Cholesterol is not uniformly distributed within the membranes and across different cellular compartments. The cytosolic leaflet of the plasma membrane is enriched with cholesterol [45]. Furthermore, the plasma membrane contains certain small microdomains with high cholesterol and sphingolipid content that are called *lipid rafts*. In neurons, membrane rafts have been detected at synapses, where they are thought to contribute to pre- and post-synaptic functions [46].

The brain contains more cholesterol than other organs. It has its own cholesterol metabolism as it is synthesized locally by different types of glial cells. However, there is a constant efflux of cholesterol from the brain, which is enabled by the neuron-specific cytochrome P450 oxidase CYP46. This enzyme hydroxylates cholesterol to 24S-hydroxylcholesterol (24-OHC), which crosses the blood-brain barrier, enters the circulation, and is metabolized by the liver [44].

1.5.2 Cholesterol-associated neurodegenerative diseases

Altered cholesterol homeostasis can lead to numerous inherited disorders with severe neurological syndromes, such as Alzheimer's disease, Huntington's disease, Parkinson's disease, Smith-Lemli-Opitz disease and Niemann-Pick type C disease [47].

Niemann-Pick type C (NPC) disease is a typical lysosomal lipid storage disorder caused by the mutations of either the NPC1 and NPC2 genes, which cause progressive visceral, neurological and psychiatric symptoms and premature death. The symptoms include delayed development of motor skills, supranuclear gaze palsy, gait problems, frequent falls, clumsiness, difficulties to speak and learn, and ataxia. The neurological disorder consists mainly of cerebellar ataxia, dysphagia, dysarthria and progressive dementia. Cataplexy, seizures, and dystonia are other common features [48].

NPC defines as a disorder characterized by abnormalities of intracellular transport endocytosed cholesterol with sequestration of unesterified cholesterol in lysosomes and late endosomes. NPC1 and NPC2 cooperate to mediate the exit of cholesterol from the endosomal-lysosomal system. In NPC cells, the physiological trafficking of cholesterol is impaired, and therefore, it accumulates within lysosomes. This anomaly constitutes the cellular hallmark of the disease. Due to this sequestration, the subsequent induction of all low-density lipoprotein (LDP) cholesterol-mediated homeostatic responses is retarded in NPC cells [48].

1.5.2.1 Cyclodextrins in NPC treatment

β-Cyclodextrin is known to bind cholesterol. It can serve as a cholesterol mopping agent due to this characteristic. The direct action of CDs on cells include the extraction of cholesterol and phospholipids, as well as some proteins from cell membranes, thereby modifying the

molecular composition of the lipid bilayers and thus their properties [49]. The mechanisms of β-CDs for modulating intracellular cholesterol homeostasis are not clear. There are several possible mechanisms that can explain the roles of CDs in cholesterol homeostasis in an NPC disease model. Either β-CDs extract cholesterol from the plasma membrane, then cholesterol from the intracellular compartments moves to the plasma membrane, replacing cholesterol that has been lost; or β-CDs enter the cell via endocytosis and directly bind and export cholesterol from the late endosomes and lysosomes [50].

The administration of a particular chemical modification of β-CD, the 2-hydroxypropyl-β-cyclodextrin (HPβCD) to *Npc1*$^{-/-}$ mice at 7 days of age has shown to prolong the lifespan, and delay neurodegeneration and lowered whole-body cholesterol content. However, when treatment was applied to older mice, the effects of CD on life duration and neuronal function recovery were significantly decreased [49]. It might be the consequence of older mice having a mature blood-brain barrier, through which CD was not able to cross efficiently. To facilitate the CD delivery directly into the central nervous system, (HPβCD) was infused intracerebroventricularly in *Npc1*-deficient mice [50].

HPβCD is internalized by cells into the lysosomes through endocytosis, where it allows the release of trapped cholesterol from the lysosome of NPC disease cells into the cytosol to be normally metabolized. HPβCD is currently in phase I/II [NCT03893071] and phase II/II [NCT03893071] clinical trials for NPC treatment [40].

Cyclodextrins and their derivatives are promising therapeutic tools in the treatment of cholesterol-associated vascular and neurodegenerative diseases [51].

1.6 Cyclodextrin-decorated superparamagnetic iron oxide nanoparticles

Superparamagnetic iron oxide nanoparticles (SPIONs) are used in an expanding number of applications in the biological field. The most common include cell labeling, contrast agents for magnetic resonance imaging, and drug delivery. For these applications, the iron oxide cores are coated with a polymer, lipid, or other dispersants to enable their dispersion in aqueous solutions containing biomolecules. The stabilizing shell is critical to avoid rapid aggregation and precipitation [52].

Nanoparticle formulations can improve the bioavailability of drugs. SPIONs are widely used in nanomedicine due to their biocompatibility and ease of functionalization. They offer great advantages in terms of stability and surface modification. On the other hand, they can

accumulate and remain within tissues for long and still undergo biocompatible degradation [53]. The decoration of SPIONs with therapeutic agents has shown superior therapeutic effects, such as decreased clearance rate, improved bioavailability and the possibility to target tissues.

SPIONs could be a novel platform to deliver CDs, improving their therapeutic efficacy for neurodegenerative disorders associated with cholesterol.

Cyclodextrin-coated superparamagnetic iron oxide nanoparticles (CySPIONs) were suggested by Puglisi *et al*. [54] for the delivery of β-CDs released from the nanoparticles at the slightly acidic pH of the lysosomes, where the build-up of cholesterol occurs. The packaging of CDs into a nanoparticle offers the advantage of suppressing renal clearance due to the increased size and thereby improving the circulation and the likelihood of endosomal targeting while potentially increasing the crossing of the blood-brain barrier.

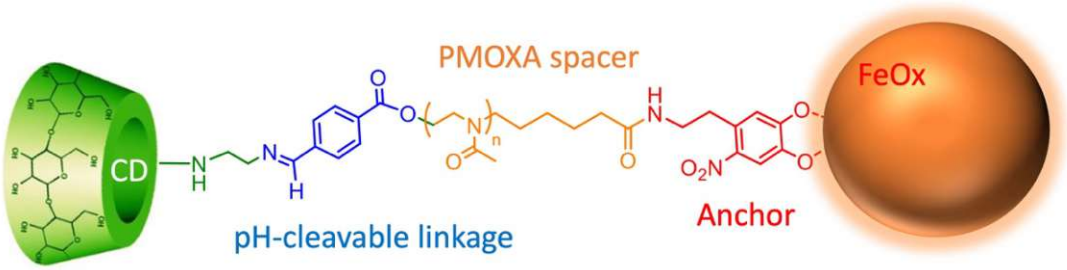

Figure 4. Schematic representation of the nanoarchitecture of CySPION

The CySPION's nanoarchitecture is schematically shown in Figure 4. The superparamagnetic iron oxide core is grafted with poly(2-methyl-2-oxazoline) (PMOXA) via a nitrodopamide anchor. PMOXA forms a dense, but highly hydrated polymer brush that colloidally stabilizes the particle and shields it from non-specific protein adsorption and unwanted biological response. PMOXA lends itself to modular synthesis and high functionalization over the more commonly used poly(ethylene glycol). It also shows lower immunogenicity because of the prevalent use of PEG in a multitude of consumer and pharmaceutical products. The βCD attachment is achieved through a pH-cleavable, benzoic imine functionality embedded into the polymer structure.

MATERIALS AND METHODS

2.1 Materials

Curcumin (from *Curcuma longa* (Turmeric), powder), Sigma-Aldrich

β-cyclodextrin, Sigma-Aldrich

Methanol, ≥ 99%, Sigma-Aldrich

Acetone, >99.5%

Dimethyl sulfoxide (DMSO), ≤ 0.02%, Sigma-Aldrich

Cholesterol, Sigma-Aldrich

Cholesterol Quantification Assay Kit, Sigma-Aldrich

Cell Meter™ Caspase 3/7 Activity Apoptosis Assay Kit, AAT Bioquest

CellTiter-Blue® Assay, Promega

Dulbecco's Modified Eagle Medium (DMEM), Gibco

GlutaMax, Gibco

HEPES, Gibco

PenStrep, Gibco

Fetal Calf Serum (FCS), Gibco

Minimum Essential Medium Eagle (MEM), Gibco

TrypLE, Gibco

Phosphate-buffered saline (PBS), Gibco

2.2 Preparation of curcumin-loaded solutions

The curcumin-β-cyclodextrin (CUR-CD) complex was obtained using a solvent evaporation method in a (1:1) molar ratio [37]. In brief, 40.5 mg β-CD was dissolved in 8 ml water (MilliQ) in a glass vial with a magnetic stirrer. 18.9 mg curcumin (representing a slight excess to the cyclodextrin) was dissolved in 500 µl acetone and added dropwise to the aqueous CD solution. The dark orange solution was left stirring overnight. The suspension was then

centrifugated at 5000 rpm for 5 min at 25 °C in order to remove the excess of curcumin and isolate the 1:1 complex in the supernatant.

CD concentration in CySPIONs was estimated to be 60 μM for a solution at 0.5 mg/ml [54]. Curcumin-loaded CySPIONs was also prepared with the solvent evaporation method

UV-Vis- and IR spectroscopy were used to confirm the formation of the complex [55].

2.3 Ultraviolet-visible absorption spectrometry (UV-Vis)

Absorption of ultraviolet (UV, 200 nm ≤ λ ≤ 400 nm) or visible (VIS, 400 nm ≤ λ ≤ 800 nm) light changes the electron distribution of molecules and atoms. Electrons jump from lower energy orbits to higher energy orbits, thereby they become excited. The part of a molecule in which electron transitions occur, meaning they absorb light are called chromophores. The rate at which light is absorbed is called the absorbance

$$A_\lambda = lg \frac{I_0}{I}$$

where A_λ is the absorbance at a given wavelength, I_0 is the intensity of the incident light and I is the intensity of the detected light. If the absorbance is measured as a function of the energy (wavelength) of the incident electromagnetic wave, an absorption spectrum is obtained. The location of absorption bands in the absorption spectra provides qualitative information [56].

UV-Vis spectra of an aqueous CUR and CUR-CD solution in 1:1 ratio were recorded using a Hitachi U-2900 Spectrophotometer.

2.4 Infrared Spectroscopy

Infrared spectroscopy is a commonly used technique for investigating materials in the liquid or solid phase. Upon interacting with electromagnetic radiation, the chemical bonds among the atoms of the matter start vibrating. For a material to absorb radiation in the infrared region, there must be resonance among the frequencies of the infrared radiation and molecular vibration. The vibration will cause the dipole moment to change. The vibration frequencies of a chemical bond are dependent on the stiffness of the given bond, and the masses of the atoms at each end of the bond. There are two main types of molecular vibrations: *stretching*, which changes the bond length, and *bending*, which changes the bond angle [57].

The absorption bands in the spectra are commonly represented by wavenumber $\tilde{v}$, expressed in cm^{-1}, because it is directly proportional to the energy (E) and frequency (ν) of radiation, according to the equation:

$$E = h\nu = \frac{hc}{\lambda} = hc\tilde{\nu}$$

where h is the Planck's constant and c is the speed of light in vacuum. The band intensity can be expressed in transmittance or absorbance. Transmittance (T) is defined as the ratio between intensities of the transmitted (I) and incident (I_0) light beams. Absorbance is the base 10 logarithm of the reciprocal of the transmittance:

$$A = log_{10}\left(\frac{1}{T}\right) = log_{10}\left(\frac{I_0}{I}\right)$$

The transmitted radiant energy is dependent on the thickness (x) and absorption coefficient (α) of the sample, according to the equation:

$$I = I_0 e^{\alpha x}$$

The spectra can be obtained by transmission or reflection method. The technique of attenuated total reflectance (ATR) operates by measuring absorptions in the reflected beam spectrum via its evanescent field close to the reflecting surface where the sample is clamped.

IR spectroscopy was used alongside UV-Vis to confirm the complexation. All materials were solid, in their powder form. To make the physical mixture, 10 mg CUR and 30.8 mg CD were mixed.

Infrared measurements were recorded on the Vertex ATR unit, and the measurements were performed with a 4 cm^{-1} spectral resolution and each spectrum is an average of 32 measurements.

2.5 Differential Scanning Calorimetry

Calorimetry is a useful technique for measuring the thermal properties of materials to establish a connection between temperature and specific physical properties of substances. There is a wide range of types of calorimeters, and differential scanning calorimeter (DSC) is a popular one. It determines the temperature heat flow associated with material transitions as a function of time and temperature. During the changing of the temperature, DSC measures the heat radiated or absorbed by the sample on the basis of a temperature difference between the sample and the reference material [58].

In terms of the mechanism of operation, DSCs can be divided into two types: heat-flux DSC and power-compensated DSC. In a heat-flux DSC, the sample material, being enclosed in a pan, and an empty reference pan are placed on a thermoelectric disc surrounded by a furnace. The furnace is heated at a linear heating rate, and the heat is transferred to the sample and reference pan through the thermoelectric disk [63]. Owing to the heat capacity of the sample, there is a temperature difference between the sample and reference pans, and the consequent heat flow is determined by the thermal equivalent of Ohm's law:

$$q = \frac{\Delta T}{R},$$

where q is the heat flow of the sample, ΔT is the temperature difference between sample and reference, and R is the resistance of the thermoelectric disk [59].

DSC spectra of the powdery form of curcumin, β-cyclodextrin, physical mixture, and curcumin-β-cyclodextrin-complex were measured. The heating rate employed was 10 °C/min in a synthetic air stream and the samples were scanned in the temperature range 25-650 °C to guarantee all material had been burnt. The thermograms were recorded with a Mettler Toledo TGA/DSC 1 STAR System.

2.6 Dynamic Light Scattering

Dynamic Light Scattering (DLS) is a photon correlation spectroscopic method and a very powerful tool for studying the diffusion behavior of molecules in solution. The diffusion coefficient, and thereby the hydrodynamic radius is calculated from it, based on the size.

During the measurement, the intensity fluctuations of scattered light are analyzed, which is due to Brownian motion of the scattering objects. Brownian motion is the random movement of particles due to the bombardment by the solvent molecules that surround them. Such motion depends on the size of the molecules, the temperature, and the viscosity of the solvent. Therefore, knowing the temperature is essential as the viscosity depends on it. Larger particles have slower Brownian motion, while smaller molecules move more rapidly. The size of the particles is calculated using the Einstein-Stokes equation:

$$d = \frac{kT}{3\pi\eta D}$$

where k is the Boltzmann coefficient (1.38×10^{-23} J/K), T (K) is the absolute temperature, η (Pa s) is the viscosity of the medium, and D (m^2/s) is the translational diffusion coefficient.

The diameter measured is a value that refers to how a particle diffuses within a fluid, so it is referred to as hydrodynamic diameter [60].

The diffusion coefficient is measured by determining the rate at which the intensity of the scattered light fluctuates when detected. This rate is dependent on the speed, hence the size of the particles. Smaller particles cause the intensity to fluctuate more rapidly than large ones. All DLS devices use a correlator, which constructs the correlation function of the scattered intensity. Sizes can be obtained from this correlation function by fitting distributions of decorrelation times to obtain the mean size (Z-average diameter) and an estimate of the width of the distributions (polydispersity index, PdI). A common fitting approach is the so-called CONTIN algorithm, which assumes a set of log-normal size distributions. The polydispersity index is obtained by the instrument and is a number between 0 and 1, showing the polydispersity of particles. The larger the particles, the more polydisperse the sample [61].

The measurement was carried out with a Malvern Zetasizer Nano instrument to determine the size- and intensity distribution of 0.5 mg/ml of aqueous CySPIONs and CUR-CySIONs (60 µM in CUR). All results are an average of 3 measurements at 25°C.

2.7 Transmission Electron Microcopy

Transmission electron microscopes (TEM) are instruments that use electron beams instead of light to image electron density contrasts in a thin sample in transmission [62]. They provide high magnification and resolution, and can be used to take images at the atomic scale. Beyond size and morphology, precise information about the crystal structures of small nanoparticles can be obtained. In addition to the morphological studies mentioned so far, TEM has life science relevance that can also be used in nanotechnology, for example, to study nanoparticle coronae or to visually represent certain cellular interactions. A drawback when applied to biological samples it is that sample has to be fixed, replicated or imaged on a cryo-stage as the measurements are performed in vacuum. Another advantage of TEM is that a little amount of sample is sufficient to obtain significant information.

Thin sections were cut of CHO cells treated with CySPIONs and studied with FEI Tecnai G^2 20 TEM instrument in order to confirm the internalization of nanoparticles into the cells.

2.8 Cell lines

Different cell lines were used to explore cholesterol-mopping properties, toxicity, apoptotic and antibacterial effects of CUR, β-CD, CUR-CD, CySPION, and CUR-CySPION.

2.8.1 Chinese hamster ovary (CHO) cells

Chinese hamster ovary cells are an epithelial cell line derived from the ovary of the Chinese hamster, often used in biological and medical research and commercially in the production of recombinant therapeutic proteins. They have found wide use in studies of genetics, toxicity, gene expression, particularly to express recombinant proteins. CHO cells are the most commonly used mammalian hosts for the industrial production of recombinant protein therapeutics [63].

CHO NPC -/- cells were donated to us by Prof. Frances Platt (Dept Pharmacology of the University of Oxford) and cultivated in our lab. In this engineered cell line, the functional role of the protein regulating cholesterol trafficking in the cell is compromised, thereby exhibiting characteristic accumulation of cholesterol in the lysosomes.

CHO cells were cultured in Dulbecco's Modified Eagle Medium (DMEM), GlutaMax and 4-(2-hydroxyethyl)-1-piperazineethanesulfonic acid (HEPES), which were supplemented with 10% fetal calf serum (FCS) and 1% antibiotics (PenStrep) at 37 °C overnight.

CHO cells were seeded in a 48-well microplate at a density of $2x10^4$ cells per well in a final volume of 400 µl in DMEM/F12 medium. After 24h the consumed medium was replaced with 200 µl fresh medium and treated with 50 µl of test samples as per Table 1-2. Other cells were left untreated as a negative control and left incubating overnight. The wells were washed with PBS once, then refilled with 400 µl medium, and incubated for 48 h.

CySPION concentration (mg/ml)	β-CD concentration in CySPION (µM)	β-CD concentration (µM)
0.1	12	12
0.2	24	24
0.5	60	60
1	120	120

Table 1. Different concentrations of CySPIONs and β-CDs applied to CHO cells

SOLUTION	Concentration of CUR (μM)	Concentration of β-CD (μM)
CUR-CD complex	60	500
CySPION	-	120
CUR-CySPION	60	120

Table 2. The concentration of components applied to CHO cells

2.8.1.1 Cytotoxicity of CDs and CySPIONs

The effects of CD and CySPION treatment on cell viability were determined using CellTiter-Blue Assay. This is a fluorometric method for estimating the number of viable cells. The assay is based on the ability of living cells to reduce the redox blue dye *resazurin* into red *resorufin*, which is highly fluorescent by the mitochondrial respiratory chain. Nonviable cells rapidly lose their metabolic capacity and do not reduce resazurin, and thus do not generate fluorescent signals [64]. The CHO NPC -/- cells were treated with 40 μl assay reagent per well. After 2 hours of incubation, fluorescence was measured at $560(20)_{ex}/595(35)_{em}$ nm at 37 °C using the TECAN Infinite F200 plate reader.

2.8.1.2 Cholesterol-mopping activity of CDs and CySPIONs

Cyclodextrins, in particular the β-CDs, are able to interact with cell membranes and are known to extract cholesterol and other lipids from the membranes. In order to assess the potential of β-CDs in cholesterol-mopping activity, the supernatants were further examined. The capacity of β-CD and CySPION to sequester cholesterol was assessed via a Cholesterol Assay Kit. The assay quantifies the cholesterol concentration through a coupled enzymatic reaction, resulting in a fluorometric measurement proportional to the cholesterol present.

To quantify the cholesterol content, a calibration curve was built using the CHO NPC -/- cells in the medium as blank. Briefly, a cyclodextrin stock solution was prepared by dissolving 22.7 mg of β-CD in 10 ml water, resulting in a 2 mM solution. 1 ml of this stock solution was separated into 6 different glass vials, all of them having the same concentration for β-CD. A cholesterol stock solution was made by dissolving 9.3 mg of cholesterol in 10 ml acetone, resulting in a 2.4 mM solution. Of this, different dilutions were made in order to achieve 2, 1.6, 1.2, 0.8, 0.4 mM stock solutions. From each of the 6 stock solutions, 50 μl was

added to the 6 vials containing the β-CD solutions in order to make solutions of 20, 40, 80, 100 and 120 µM concentrations for cholesterol. All 6 samples were stirred overnight, to form cholesterol-cyclodextrin inclusion complexes with the solvent evaporation method.

The fluorescence measurement was carried out using Infinite F200 microplate reader. In a 96-well plate duplicates were prepared using 25 µl blank and 25 µl of the respective cholesterol-cyclodextrin complex was added in order to make 0, 5, 10, 15, 20, 25, 30 µM solutions for the calibration curve (Figure 5).

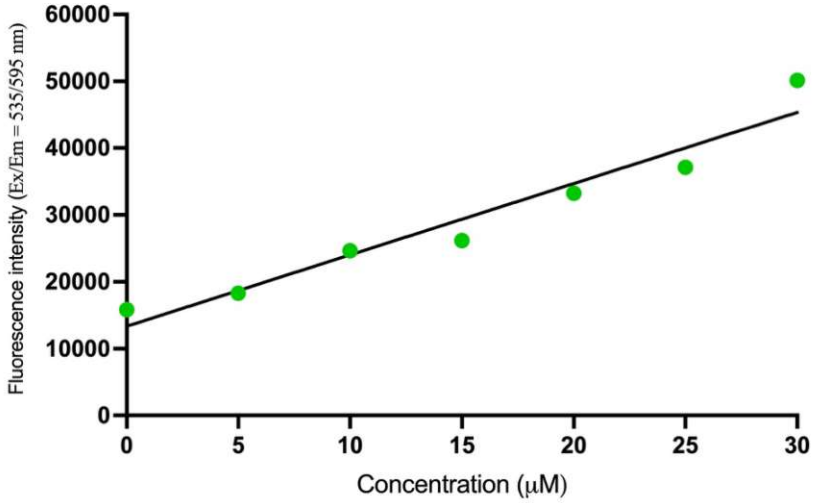

Figure 5. Calibration curve for the cholesterol-mopping activity study

The cholesterol content of the supernatants was determined as per kit protocol. A 50 µl reaction mix was added to 50 µl of samples per well. After 30 minutes of incubation at 37 °C, the fluorescence was measured at Ex/Em = 535(25)/595(35) nm using Infinite F200 plate reader.

2.8.1.3 Cellular uptake

Nanoparticle cellular uptake was studied with TEM through cellular embedding. Pelleted cells were fixed in standard fixative (2% formaldehyde and 2.5% glutaraldehyde in 0.1 M cacodylic acid buffer of pH 7.4) for 1 h. After centrifugation, the supernatant was discarded and the pellet was embedded in 1 drop of 2% agarose, then cut into strips. The fixation was continued with a standard fixative containing 1% tannic acid for 2 h. The samples

were washed 3 times with buffer, followed by 2 washes in MilliQ water. Then, they were fixed with 1% osmium tetroxide (OsO_4) in 1.5% K-Hexacyanoferrate (III) for 2 h, and 1% OsO_4 in MilliQ for an additional 1 h. After that, the cells were washed again 5 times with MilliQ. Following this, a dehydration process was started with graded ethanol series (70%, 80%, 90%, 2x100%) for 10 minutes each. The resin was prepared by mixing equal amounts of Embed-It® solutions. For infiltration, the samples were incubated for 1 h in LR-White. Then, the resin was changed and incubated overnight at 4 °C. Following incubation, sample stripes were transferred to gelatin capsules, filled up with fresh resin and polymerized for 24 h at 60 °C. Blocks in quarters were cut and thin sections were prepared at the Ultracut (~70 nm).

2.8.2 HepG2 cells

HepG2 is a human hepatoma that is commonly used in drug metabolism and hepatoxicity studies. This cell line was derived from liver biopsies of a 15-year-old Caucasian male with a differentiated hepatocellular carcinoma. They are nontumorigenic cells with high proliferation rates and an epithelial-like morphology that perform many differentiated hepatic functions [65].

As discussed, curcumin can be toxic to cells. HepG2 cells were cultivated to examine the apoptotic properties of free curcumin, and curcumin-loaded cyclodextrins and SPIONs through CellTiter-Blue viability assay and Cell Meter Caspase 3/7 Activity Apoptosis Red Fluorescence Assay Kit. The kit is designed to monitor cell apoptosis through Caspase 3 activation, which is important in the initiation of apoptosis. Caspase 3 has substrate selectivity for the peptide sequence Asp-Glu-Val-Asp (DEVD). The cleavage of the DEVD blocking peptide residue by caspase 3 generates a red fluorescent signal [66].

HepG2 cells were cultured in Minimum Essential Medium Eagle (MEM), GlutaMax, Earle's salts, 25 mM HEPES and 1x MEM-vitamins, supplemented with 10% FCS and 1% antibiotics (PenStrep). Cells were washed with phosphate-buffered saline (PBS) and detached with 5 ml TrypLE, centrifugated, and resuspended in 5 ml medium.

The apoptosis response of HepG2 cells to free curcumin, CUR-CD complex and CUR-CySPION were analyzed by the apoptosis assay. Briefly, HepG2 cells were seeded in 3 different microplates at a density of $4x10^4$ cells per well in a final volume of 200 µl. After 24 h, the medium was removed and the cells were treated with 50 µl of CUR (in DMSO), CUR-CD, CUR-CySPION in 200 µl final volume as stated in Table 3, for 6, 24 and 48 h. The DMSO

content was kept at 0.15% in an effort not to affect cells. At the time of the analysis, the medium was replaced, and an equal amount of Z-DEVD-ProRed Reagent Assay was added to each well. Following incubation of cells at room temperature for 1 h in the dark, the fluorescent intensity at Ex/Em = 535(25)/635(35) nm was monitored by Infinite F200 plate reader.

SOLUTION	Concentration of CUR (μM)	Concentration of CD (μM)
CUR	60	-
CUR-CD complex	60	300
CUR-CySPION	60	120

Table 3. The concentration of test samples introduced to HepG2 cells

2.8.3 *Staphylococcus aureus*

Staphylococcus aureus is a cocci-shaped Gram-positive bacterium that tends to be arranged in clusters that are described as "grape-like". It is found in the environment and is also in normal human flora, located on the skin and mucous membranes (most often the nasal area) of most healthy individuals. Normally it does not cause infection on healthy skin; however, it is classified as an opportunistic pathogen, which if it is allowed to enter the bloodstream or internal tissues, these bacteria may cause a variety of potentially serious infections. The most common infections include bacteremia, infective endocarditis, skin and soft tissue infections, pulmonary infections (e.g., pneumonia), gastroenteritis, meningitis, toxic shock syndrome, and urinary tract infections [67].

Mechanisms for evasion of the host immune response include the production of an antiphagocytic capsule, sequestering of host antibodies or antigen masking by Protein A, or biofilm formation [68]. The binding of the bacteria to extracellular matrix proteins and fibronectin in infectious endocarditis is mediated by bacterial cell wall-associated proteins such as fibrinogen-binding proteins, clumping factors, and teichoic acids. Prosthetic device infections are often mediated by the ability of *S. aureus* strains to form biofilms as well as communicate using quorum sensing in a bacterial cell density-dependent manner [69].

We aimed to determine the *minimum inhibitory concentration* (MIC) and *minimum bactericidal concentration* (MBC) of free curcumin, curcumin-loaded cyclodextrin, and free β-cyclodextrin against *S. aureus*.

2.8.3.1 Bacterial culture

The *Staphylococcus aureus* ATCC 12598 (DSM 20372) was obtained from the DSMZ-German collection of microorganisms and cell culture GmbH. Overnight culture of *S. aureus* was prepared by transferring a single colony from agar plate to 10 ml tryptic soy broth (TSB) in a 50 mL Erlenmeyer flask. The bacterial suspension was incubated overnight at 37 °C under shaking at 100 rpm. The bacterial culture was harvested by centrifugation at 5000 rpm for 5 minutes, and the pellet was resuspended in 10 ml fresh TSB medium. The concentration was adjusted to a dilution of 0.1 OD at 600 nm in fresh TSB by spectrophotometer.

2.8.3.2 MIC & MBC determination

Five stock solutions were made: a 271.5 µM (0.1 mg/ml) and a 3393 µM (1.25 mg/ml) CUR (in DMSO), a 1357 µM (1.5 mg/ml) and a 10.5 mM (12 mg/ml) β-CD (in H_2O) and CUR-CD in 1:5 ratio (271.5 µM for CUR and 1357 µM for β-CD) stock solution.

A broth dilution method [70] was used to study the antibacterial efficacy of the abovementioned samples by evaluating the visible growth of bacteria in TSB broth. Serial two-fold dilutions of samples in concentrations ranging according to Table 4 and 5 were used to determine MIC in TSB broth. The control contained only inoculated broth. The samples were incubated for 24 h at 37 °C and the absorbance was measured at 595 nm. The MIC was determined from the visual observation and no turbidity was noted as MIC value.

After the MIC determinations, aliquots of 50 µl from all the tubes which show no visible bacterial growth would be seeded on TSB agar plates and incubated for 24 h at 37 °C. When 99.9% of the bacterial population is killed at the lowest concentration of the antibacterial agent, it is termed as MBC endpoint.

Dilution of solutions	1	2	3	4	5	6	7	8	9	10
CUR (µM)	271.5	135.75	67.875	33.94	16.9	8.48	4.24	2.12	1.06	0.53
(mg/ml)	0.1	0.05	0.025	0.0125	0.0062	0.0031	0.0015	0.0007	0.0004	0.0002
CUR-CD	271.5	135.75	67.875	33.94	16.9	8.48	4.24	2.12	1.06	0.53
(µM)	1357	678.5	339.25	169.625	84.812	42.4	21.2	10.6	5.3	2.625
β-CD (µM)	1357	678.5	339.25	169.625	84.8125	42.4	21.2	10.6	5.3	2.625
(mg/ml)	1.5	0.75	0.375	0.1875	0.093	0.046	0.023	0.023	0.012	0.006

Table 4. Dilution of samples used for MIC determination

The measurement was repeated with further investigating in CUR and CD. A 2.5 mg/ml CUR (in DMSO) and a 12 mg/ml β-CD (in H_2O) stock solutions were prepared.

Dilution of solutions	1	2	3	4	5	6	7	8	9	10
CUR	3393	1696.5	848.25	424.125	212	106	53	26.5	13.25	6.63
(µM)	1.25	0.625	0.312	0.156	0.078	0.039	0.019	0.009	0.004	0.002
(mg/ml)										
β-CD	10.5	5.25	2.625	1.312	0.656	0.328	0.164	0.082	0.041	0.02
(mM)	12	6	3	1.5	0.75	0.375	0.1875	0.0937	0.0468	0.0234
(mg/ml)										

Table 5. Dilution of samples used for MIC determination

RESULTS AND DISCUSSION

3.1 Complex formation

3.1.1 IR-and UV-Vis spectra

IR-and UV-Vis spectroscopy was used to confirm the formation of CUR-CD inclusion complex. Curcumin's IR spectrum (Fig 6a), shows no bands in the 1800-1650 cm^{-1} region which is the most significant carbonyl region, indicating that curcumin exists in the keto-enol tautomeric form. Some prominent peaks appeared at 3505 cm^{-1} indicating the phenolic O-H stretching vibration, 1627 cm^{-1} for benzene ring stretching vibration, and 1506 cm^{-1} for C=O stretching.

β-cyclodextrin's spectrum (Fig 6b) shows -OH stretching vibration at 3290 cm^{-1} and -CH_2 stretching vibration at 2975 cm^{-1}. The characteristic band at 1022 cm^{-1} is assigned to the stretching vibration of C-O-C.

The IR spectrum of the physical mixture between CD and CUR (Fig 6c) shows the characteristic absorption peaks of both curcumin and β-cyclodextrin.

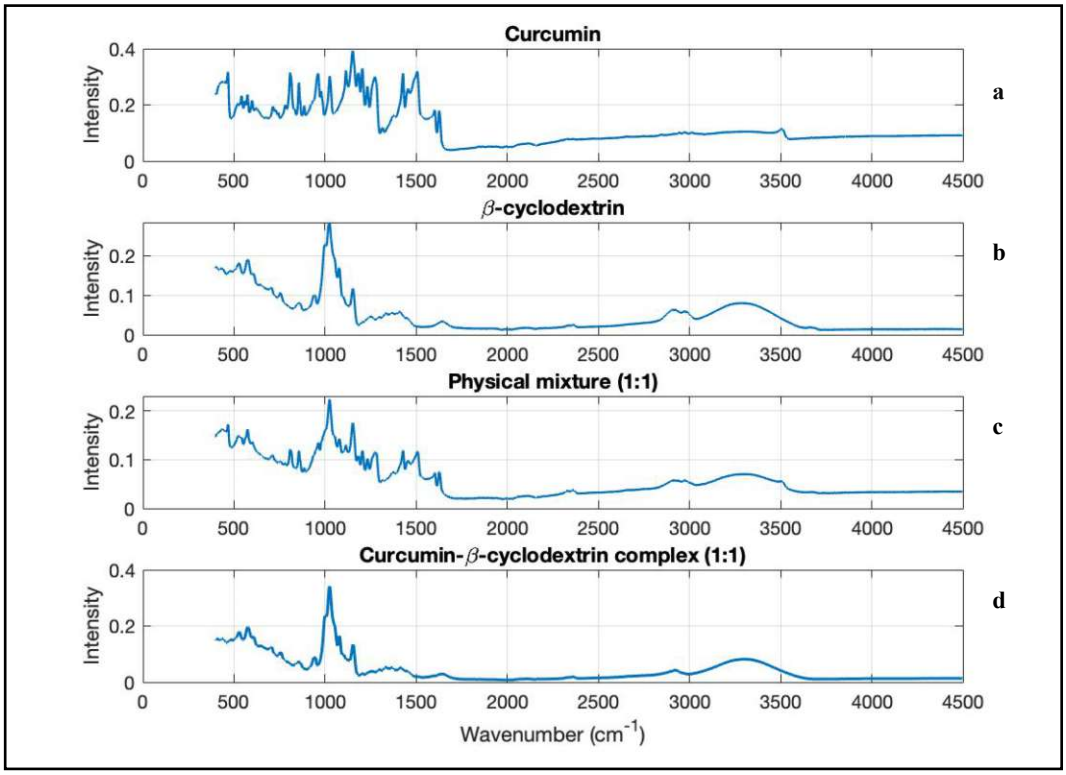

Figure 6. IR spectra of curcumin (a), β-cyclodextrin (b), physical mixture (c) and curcumin-β-CD-complex (d)

However, when the curcumin-β-CD-complex is formed, the IR spectrum (Fig 6d) shows all absorption peaks of cyclodextrin, while all the characteristic peaks of curcumin disappeared. This corresponds to the expectation from reports in the literature [55] regarding the IR spectrum of curcumin-β-cyclodextrin-inclusion-complex obtained via solvent evaporation.

The UV-Vis spectrum for the complex with the absorbance of CUR at 425 nm (Figure 7) also supports the formation of the inclusion complex.

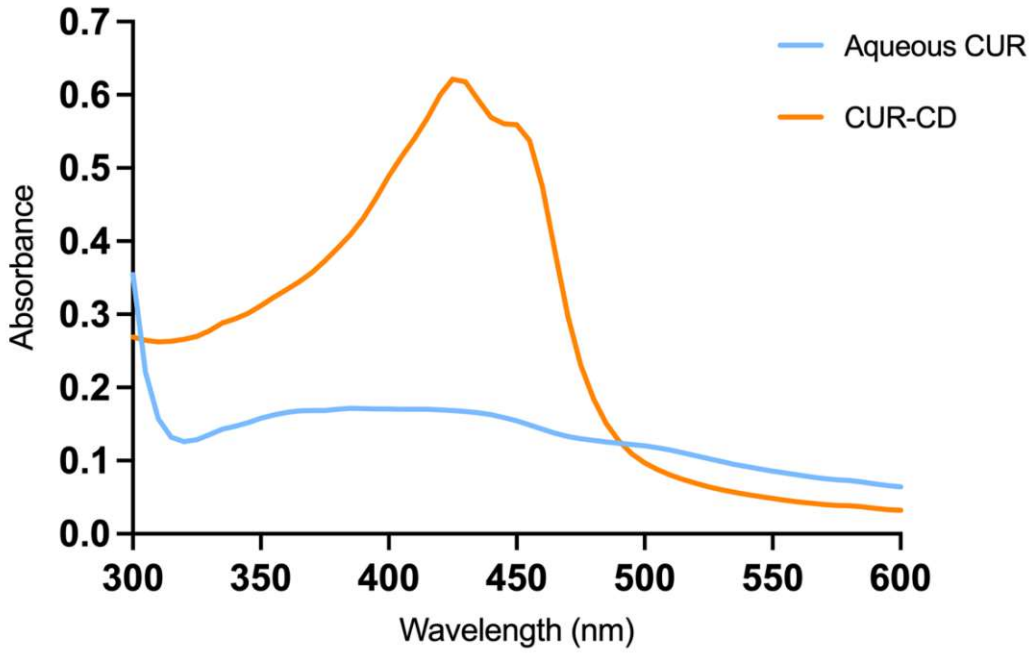

Figure 7. UV-Vis absorbance spectra of curcumin in complex and water

3.1.2 Thermograms from Differential Scanning Calorimetry

Further study of CUR, β-CD, physical mixture and CUR-CD with DSC was perform to confirm the complex formation. Individual thermograms are shown in Figure 8-11.

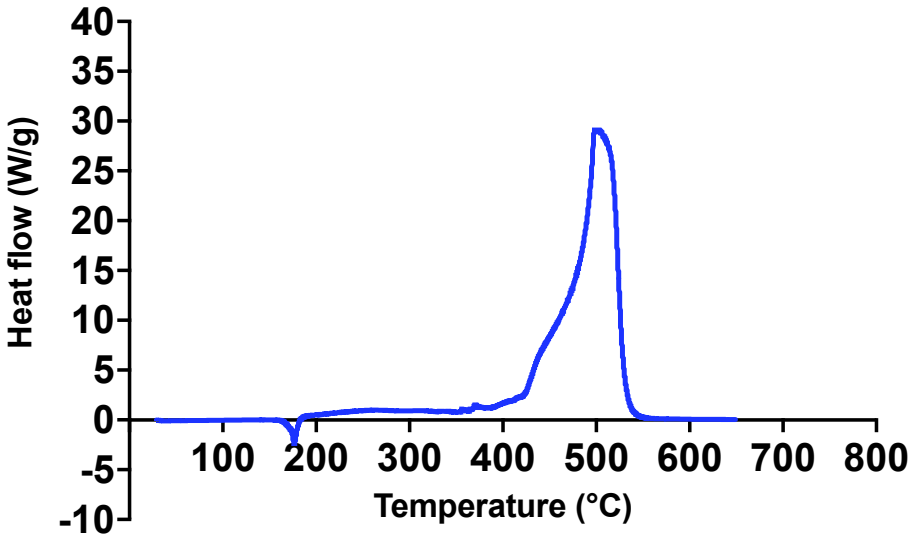

Figure 8. DSC thermogram of CUR in synthetic air stream

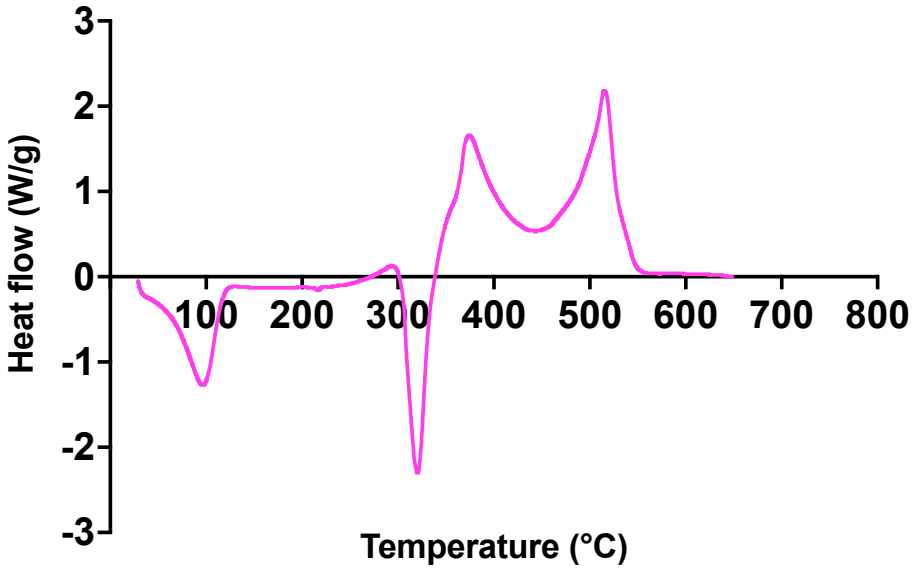

Figure 9. DSC thermogram of β-CD in synthetic air stream

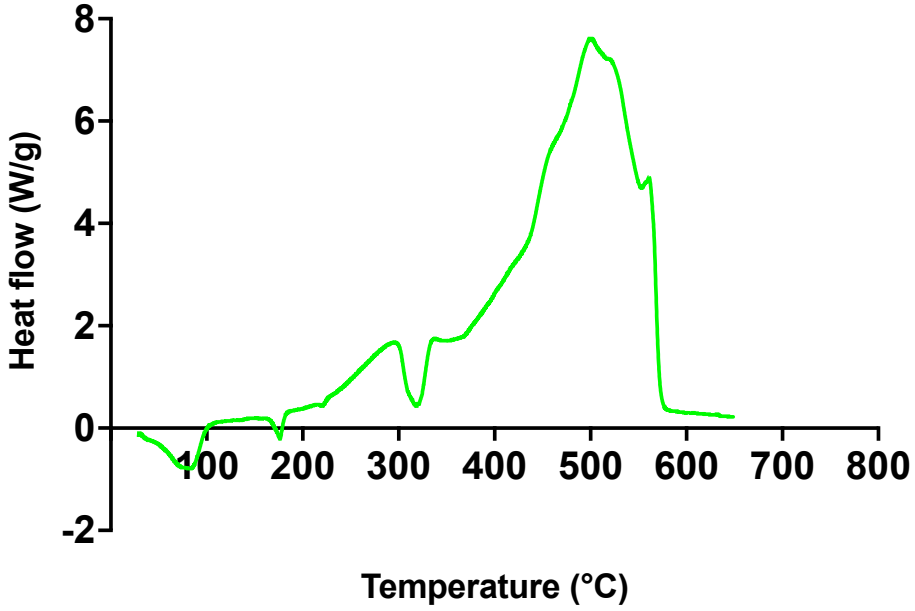

Figure 10. DSC thermogram of physical mixture in synthetic air stream

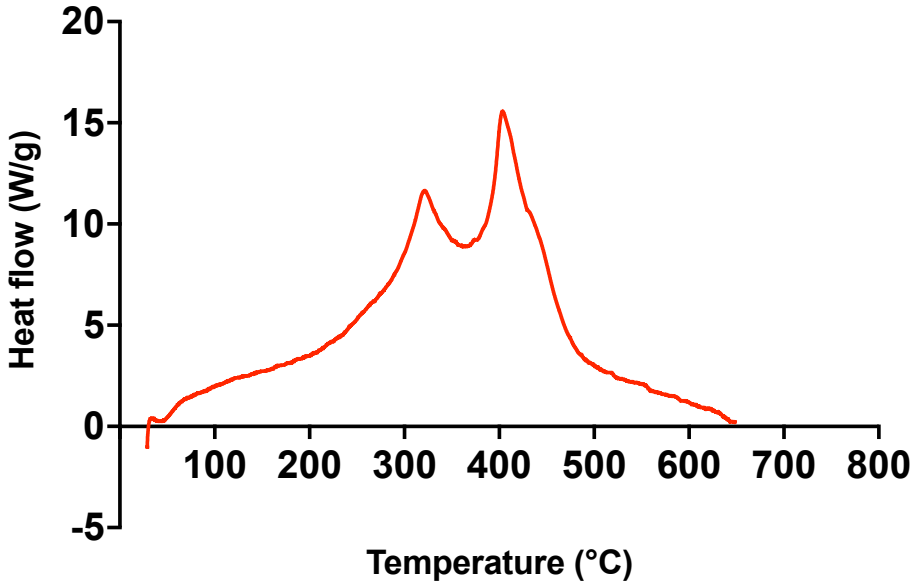

Figure 11. DSC thermogram of CUR-CD in synthetic air stream

Curcumin showed an endothermic peak at 183 °C, corresponding to its melting point [71], and a sharp exothermic peak at 510 °C, at which the material combusts. Cyclodextrin shows endothermic peaks at ~100 °C and ~320 °C. The latter is attributed to the melting temperature of β-CD, while a peak ~100 °C or ~150 °C is often observed in β-CD DSC spectra

but is unattributed. Two characteristic exothermic peaks also appeared at 380 and 520 °C, which might correspond to the combustion of different parts of the β-CD [72]. The thermal profile of the physical mixture was expected to be similar to a combination of curcumin and cyclodextrin. Deviations could occur, e.g., in terms of the observed melting temperatures, as these can even differ significantly if a true mixture is formed, with eutectic mixtures being the extreme case. In our case, the DSC spectrum of the physical mixture was mainly a superposition of the DSC spectra of the individual components, with endothermic peaks at ~100 °C, ~180 °C, and ~320 °C and a dominating exothermic peak at ~510 °C with shoulder peaks. In contrast, the inclusion complex showed neither the melting nor the combustion peaks characteristic of curcumin. Instead, only two strong exothermic peaks (at 327 and 407 °C) and a pronounced shoulder peak at a higher temperature dominate the DSC spectrum of the complex. They do not correspond to the combustion peaks for any of the individual compounds, but could be the three combustion peaks shifted to lower temperature for the complex. The strong changes in the DSC spectrum and in particular the absence of characteristic melting transitions that would only occur for individual compounds demonstrate that in a β-cyclodextrin-curcumin complex, curcumin is shielded by β-CDs. These data should confirm the formation of the inclusion complex.

3.2 Size distribution of nanoparticles

Dynamic Light Scattering (DLS) was used to determine the size distribution of both empty CySPIONs and curcumin-loaded CySPIONs (CUR-CySPION).

Figure 12 shows the size distribution of CySPIONs and CUR-CySPION by number. The Z-average of CySPION was 210.7 nm, and the PdI was 0.243, indicating a slight aggregation of the CySPIONs that were well dispersed. When curcumin is loaded into the cavities of cyclodextrin (CUR-CySPION), the Z-average becomes 663.3 nm and the PdI 0.714, indicating that upon the formation of the inclusion complex the nanoparticles tend to aggregate. This could for example occur via dimerization in the binding of curcumin between CD belonging to different CySPION.

Figure 13-14 show the size distribution of CySPION and CUR-CySPION by intensity. Fig. 13 indicates that 98.8% of CySPION having their diameter at around 210 nm. However, the intensity distribution of CUR-CySPION shows 3 peaks, having 20.1% of nanoparticles at

around 105 nm, 37.1% at ~203 nm and 42.8% at ~355 nm. This data further supports the tendency of nanoparticles to aggregate once loaded with CUR.

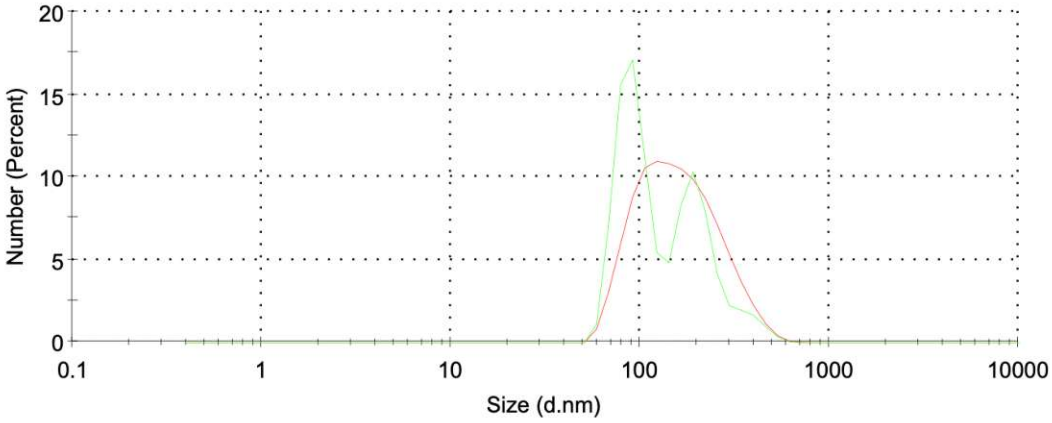

Figure 12. Size distribution by number of CySPIONs (red), and CUR-CySPIONs (green).

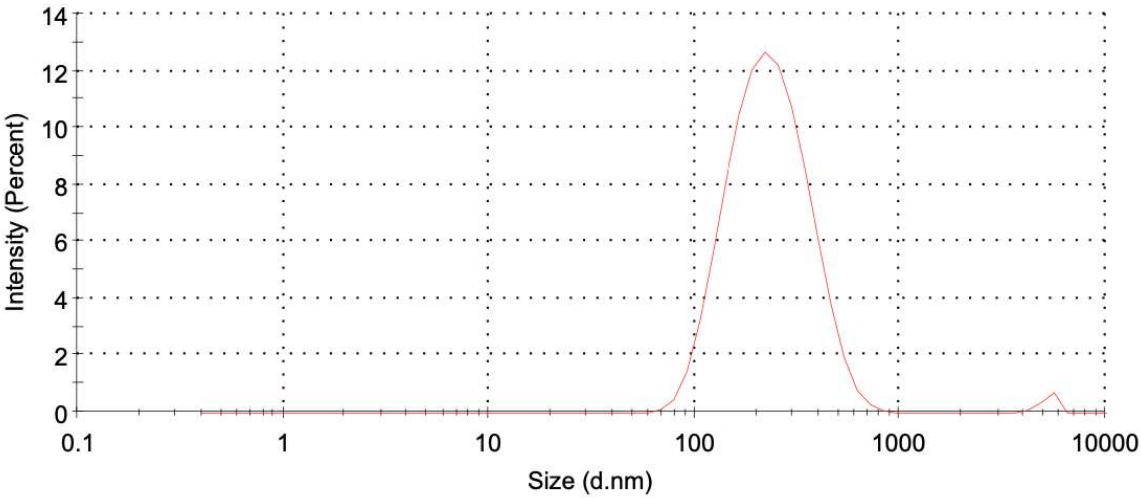

Figure 13. Size distribution by intensity of CySPIONs

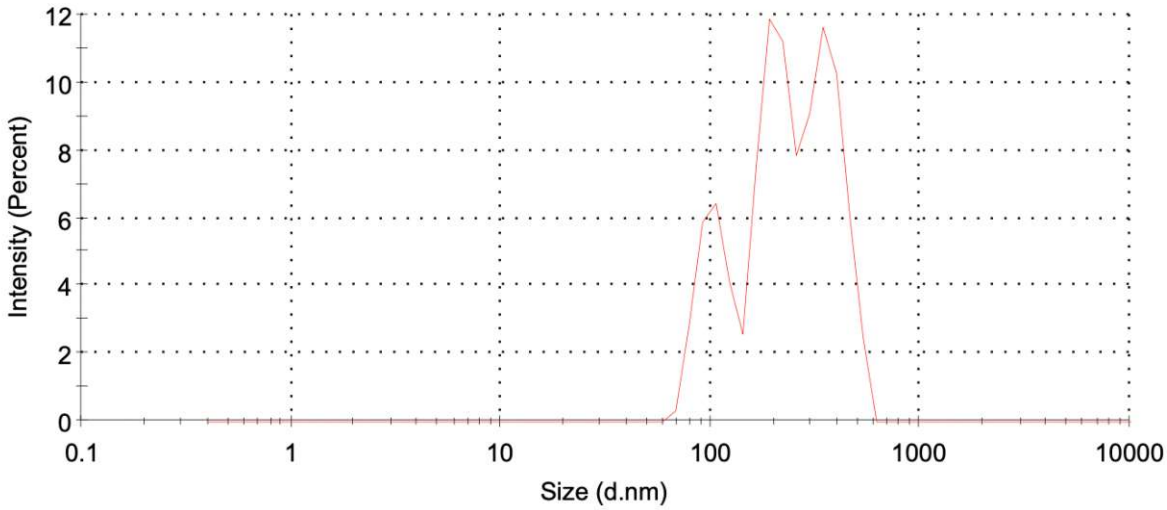

Figure 14. Size distribution by intensity of CUR-CySPION

3.3 Cholesterol-mopping activity studies on CHO NPC cells

3.3.1 Viability tests on CHO NPC cells

Cytotoxicity of monomeric β-CDs, CySPIONs, and different curcumin delivery systems were investigated on CHO NPC -/- cells after exposure for 48 h (Figure 15-16). Cell viabilities are given in percentages relative to untreated cells. Figure 15 shows the percentage of viable cells after treatment with the respective concentrations of monomeric β-CDs and CySPIONs. In the explored high range of concentrations, β-CDs and CySPIONs did not cause significant cytotoxic effects in the CHO cell line.

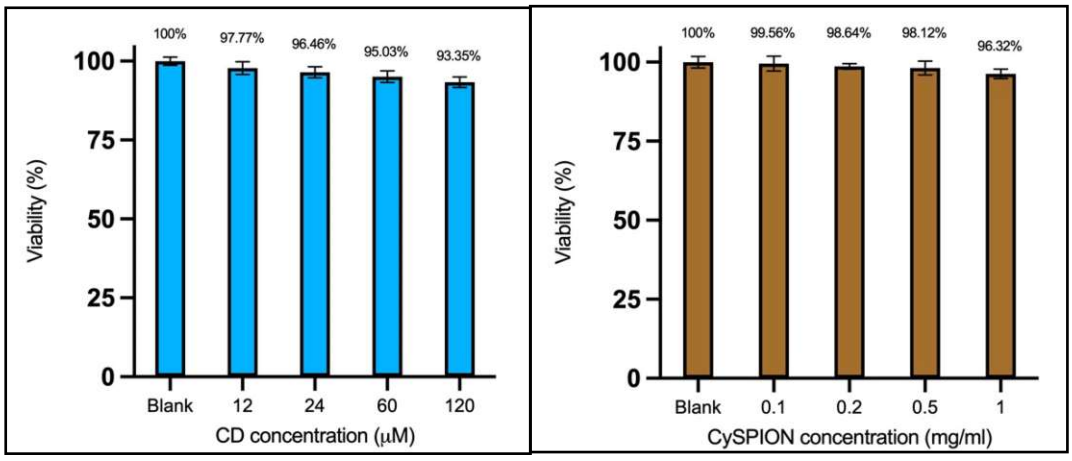

Figure 15. Viability of CHO cells treated with the respective concentration of CDs or CySPIONs for 48 h according to Table 1

Figure 16 shows cell viability when treated with curcumin-loaded CDs and CySPIONs compared to empty CySPIONs. As stated before, CUR can be toxic to cells. Although, when loaded into the carrier systems, no significant toxicity occurred. If curcumin is efficiently entrapped in the β-CD, it should not show any short-term toxic effects, which is in agreement with our results. It suggests that the CUR-CD affinity and assay times might need tuning to achieve the potential of the CUR-CD delivery system and demonstrate its effect on cells.

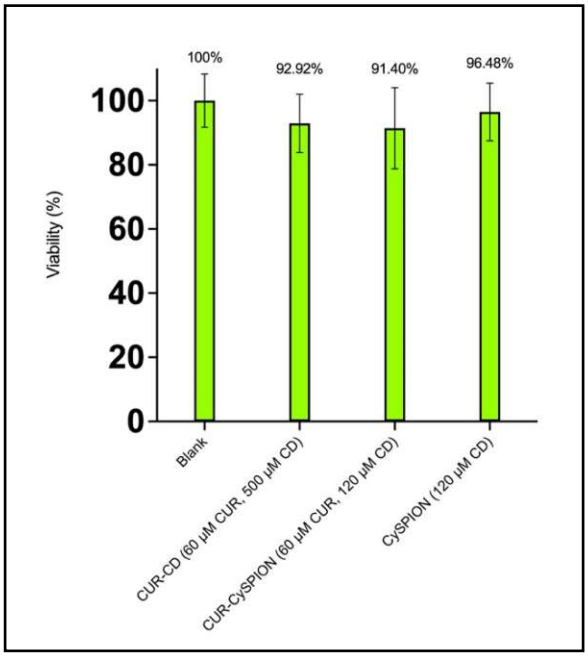

Figure 16. Viability of CHO cells treated according to Table 2 for 48h

3.3.2 Quantification of solubilized cholesterol

β-cyclodextrin's ability to form inclusion complexes with cholesterol in the lysosome could compensate for the dysfunction of cholesterol transport proteins. With this in mind, we tested the ability of the β-CD-functionalized CySPION to remove cholesterol from cells by measuring solubilized cholesterol into the supernatant on CHO cells incubated with CySPIONs via an enzymatic kit. After 24h of seeding, the cells were treated with CySPION test samples as per Table 1-2 (introduced in section 2.8.1). After 48 h incubation, the supernatants of CHO cells were treated according to the enzymatic kit assay protocol, and cholesterol concentration assessed via fluorescence (Figure 17-18).

Cholesterol content was quantified based on the calibration curve (Fig 5., section 2.8.1.2). The amount of solubilized cholesterol is determined in comparison to the blank. When

comparing CySPIONs in concentrations ranging from 0 to 1 mg/ml, to monomeric β-CDs, respective to the β-CD concentration attached to SPIONs (12-120 µM) (Figure 17), free β-CDs showed a higher level of activity in solubilizing cholesterol than CySPIONs at the same concentration. Both β-CDs and CySPIONs alone showed a concentration-dependent cholesterol modulation: the higher the concentration of applied β-CDs and CySPIONs, the higher the quantified solubilized cholesterol.

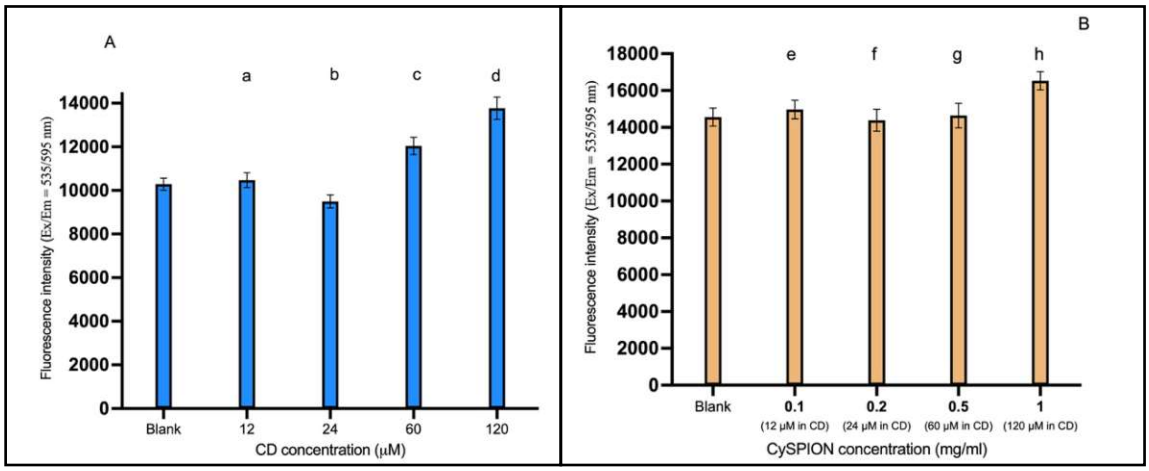

Figure 17. Fluorescence intensity of monomeric CDs and CySPIONs at different concentrations after 48 h incubation applied on CHO cells according to Table 1

Calculated cholesterol content, compared to the blank in each case: A: 0.16 µM (a), -0.7 µM (b), 1.53 µM (c), 3.04 µM (d); B: 0.36 µM (e), -0.14 µM (f), 0.07 µM (g), 1.72 µM (h)

We also studied curcumin-loaded CySPIONs and CDs, in comparison to the empty carrier counterparts for their capacity to solubilize cholesterol (Figure 18). We found that empty CySPIONs had a better cholesterol-mopping activity in comparison to the same system where its CD cavities were occupied by CUR. As in the latter case, the CUR must be expelled by the cholesterol, this underlines once more the role of CDs in the solubilization of cholesterol. We also tested the cholesterol mopping for CUR-CySPION compared to CUR-CD, where the CUR-CD concentration was ~4 times higher than the CUR-CySPION to find that in the monomeric form the CD complexes have a lower cholesterol-mopping activity (Figure 18). This finding is probably explained by the lower cellular uptake of the monomeric CD compared to the nanoparticle formulation.

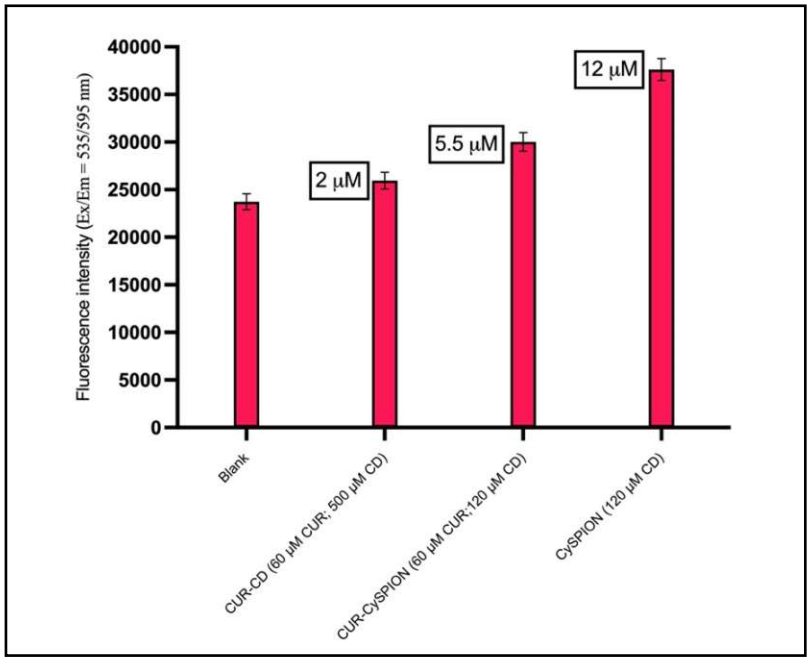

Figure 18. Fluorescence intensity of CySPION and curcumin-loaded CD and CySPION after 48 h incubation applied on CHO cells according to Table 2

3.3.3 Cellular uptake and localization of CySPIONs

TEM investigation revealed the cellular uptake of CySPIONs in CHO NPC cells (Fig. 19) through embedding, after 48 h of incubation. We could identify nanoparticle aggregates inside the cell. (Figure 19 B, C, and D show the same cluster of nanoparticles under different magnifications). Similar structures outside the cell were also detected. Presumably, they adhered to the cell membrane (Fig. 19A). These images suggest that 48 h of incubation is not efficient for good internalization; the majority of nanoparticles are still outside of the cell.

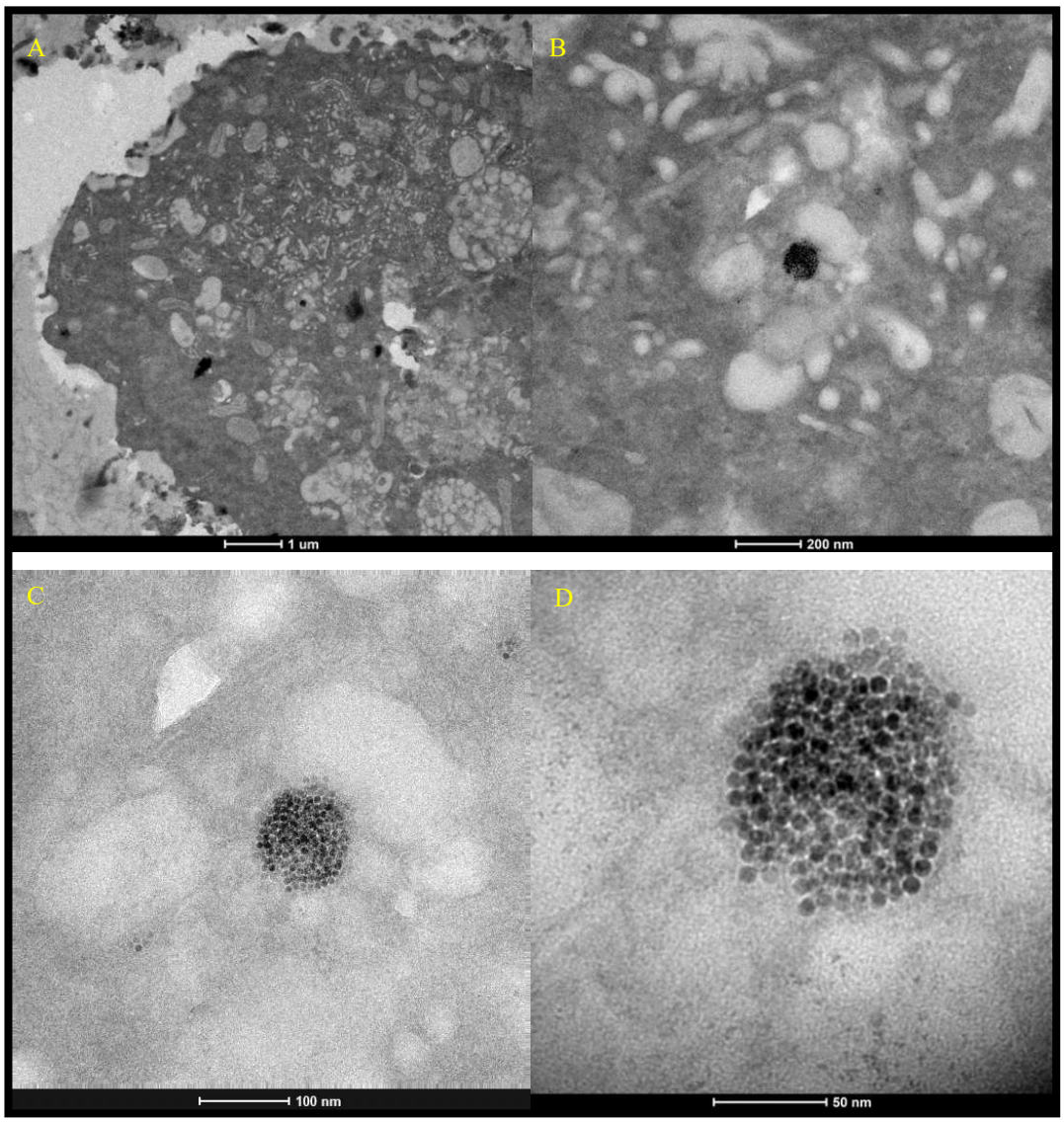

Figure 19. Cellular internalization of CySPIONs in CHO NPC cells after 48 h incubation under transmission electron microscopic view (A, B, C, and D are the microscopic view of the same object under different magnification).

3.4 Cytotoxicity and apoptotic studies on HepG2 cells

3.4.1 Viability of HepG2 cells

The cytotoxicity of free curcumin and the curcumin-delivery systems was examined on HepG2 cells with CellTiter Blue assay after treatment of 48 h as described in Table 3. Cell viabilities are given in percentages relative to untreated cells. Figure 20 shows the percentage of viable cells after treatment with the respective concentrations of free CUR, CUR-CD and CUR-CySPION.

Curcumin appeared to be highly toxic for HepG2 cells at the given concentration of 60 µM, even when keeping the DMSO content at 0.15%. Both CUR-CD and CUR-CySPION seem to be fairly cytotoxic for HepG2 cells at the respective concentrations after 48 h.

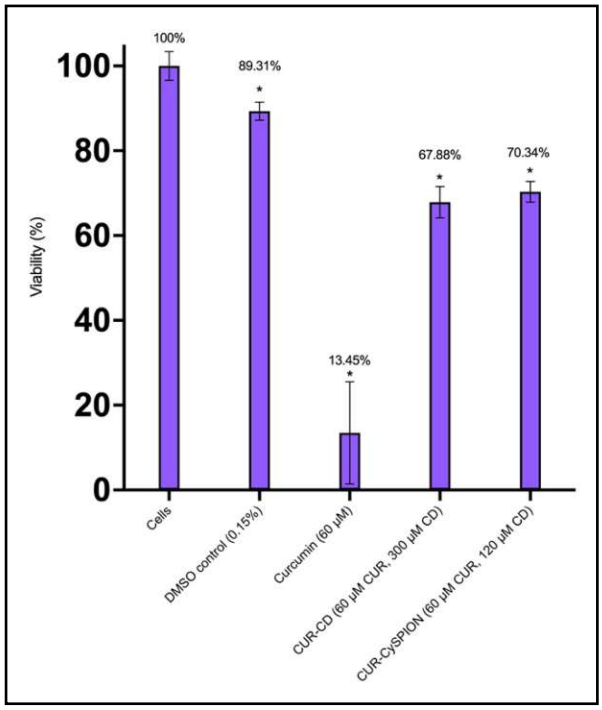

Figure 20. Viability of HepG2 cells after 48 h of exposure according to Table 3. All data were obtained from twelve measurements and three repeats on each sample are presented as means ± SD. $p < 0.05$(*) vs. control group (Cells)

3.4.2 Apoptosis-triggering response of curcumin on HepG2 cells

The apoptotic response of HepG2 cells to the samples stated in Table 3 was analyzed by a Caspase 3/7 activity assay in which higher fluorescence intensities correspond to a higher level of apoptosis (Figure 21).

After the earliest measurement point at 6h, CUR had the biggest influence on apoptosis compared to the blank, CUR-CD and CUR-CySPION barely showed any effect. CUR seemed to be more effective after 24 h. While CUR-CySPION still showed no effect, CUR-CD showed some indication of induced apoptosis. CUR started to lose its activity after 24 h, although it showed effect at later times. It indicates that free curcumin has a time-dependent effect on apoptosis, being the most effective in the first 24 h, which is comparable to other studies [73].

CUR-CD is more effective in the long term, which suggests curcumin needs longer times to get released from the cavities. CUR-CySPION started inducing significant excess apoptotic response after 48 h, suggesting the uptake of nanoparticles and the release of curcumin takes longer for CySPION than for CD.

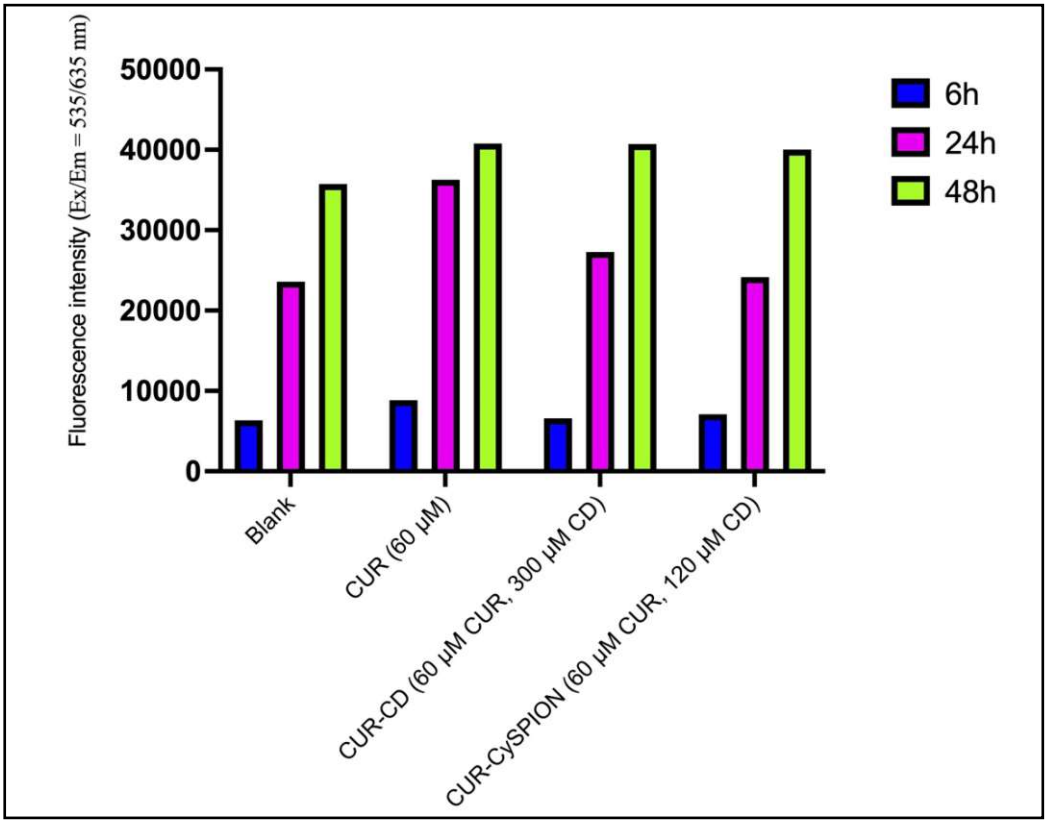

Figure 21. Apoptotic response of test substances at given times

The mechanism underlying the effects of curcumin inhibiting cancer cell growth by activation apoptosis is still unclear. Moustapha *et. al* investigated the mechanisms leading to apoptosis in curcumin-treated cells [74]. Curcumin can induce endoplasmic reticulum stress, causing calcium release which destabilizes the mitochondrial compartment, resulting in apoptosis. They have also found that lower curcumin concentrations induced apoptosis, whereas as the curcumin concentration was increased, apoptosis was progressively replaced with necrosis, probably because of the cytotoxicity of curcumin at higher concentrations.

3.5 Determining the minimum inhibitory concentration against S. aureus

A broth dilution method was used to study the antibacterial efficacy of free CUR (in DMSO), free CD and CUR-CD by evaluating the visible growth of bacteria in the microplate wells. Serial two-fold dilutions of samples in the concentration range in Tables 4 and 5 were used to determine the MIC. The samples were incubated for 24 h at 37 °C and the absorbance was measured at 595 nm using Infinite F200 plate reader.

The effect of CUR on bacterial growth is shown in Figure 22. Molarities ranging from 212 µM (0.078 mg/ml) to 3393 µM (1.25 mg/ml) CUR showed no inhibitory effects. However, CUR molarity of 135.75 µM (0.05 mg/ml) and higher caused a lag in bacterial growth. Further diluted curcumin neither inhibited nor delayed growth. The CUR-CD showed no effect on bacterial growth (Figure 23), and the trendline of growth was similar to the control. It indicates that the curcumin affinity to cyclodextrin prevented the curcumin to be released from the cavities at a sufficient rate during the period of time investigated to reach an antimicrobial concentration in the sample. However, free cyclodextrin (Figure 24) had the most significant outcome on the inhibition, yet there was visible turbidity in each well, thereby the minimum inhibitory concentration could not be determined. It is possible that β-CD can form inclusion complexes with such signal molecules, which are present for microorganisms in order to coordinate their activities. With the molecular encapsulation of these signals, their binding to receptors can be prevented, thereby reducing the communication (quorum quenching) [75].

To determine the MBC, 50 µl aliquots from the tubes with the first four higher concentrations (0.0125-0.1 mg/ml CUR; 0.15625-1.25 mg/ml CUR; 0.1875-1.5 mg/ml CD; 1.5-12 mg/ml CD) were seeded on TSB agar for 24 h at 37°C. As expected, bacterial growth was visible at all concentrations, confirming these concentrations are too low to cause growth inhibition, especially bactericidal.

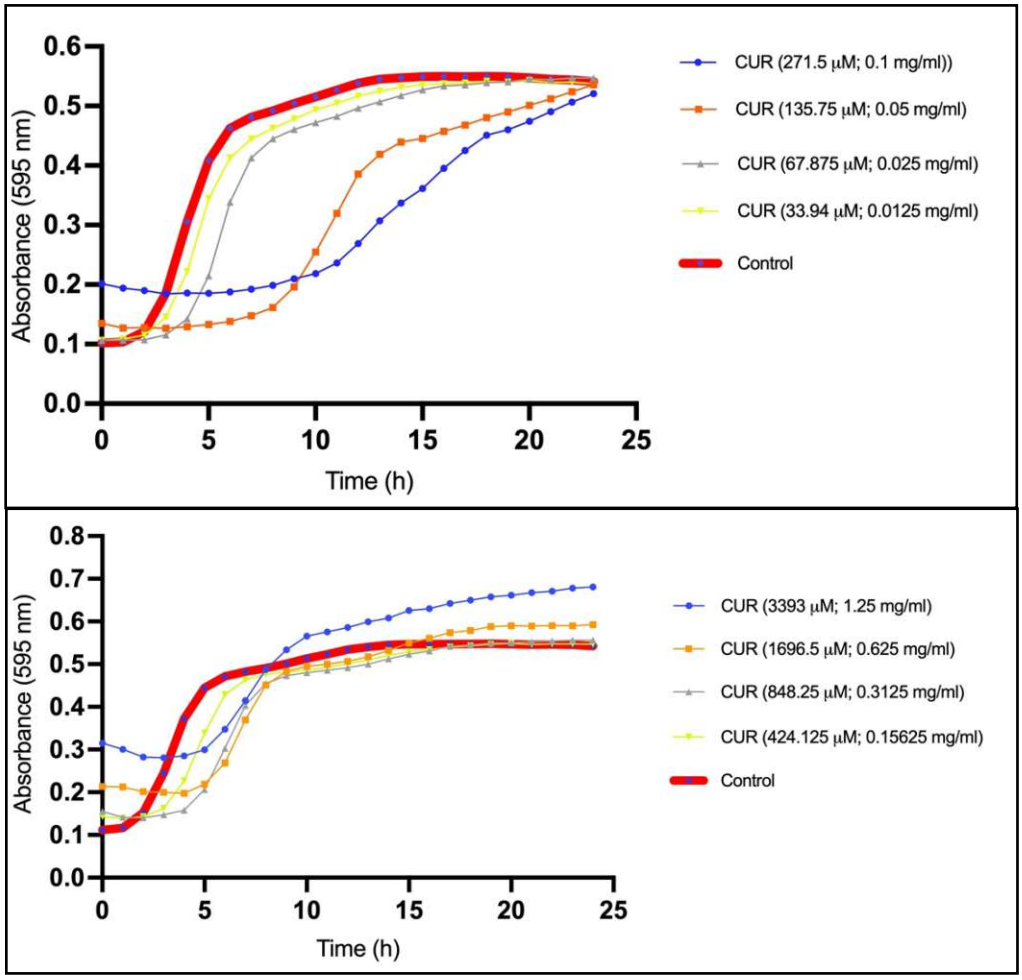

Figure 22. Bacterial growth in TSB broth, incubated for 24 h at 37 °C, after applying free curcumin at different concentrations

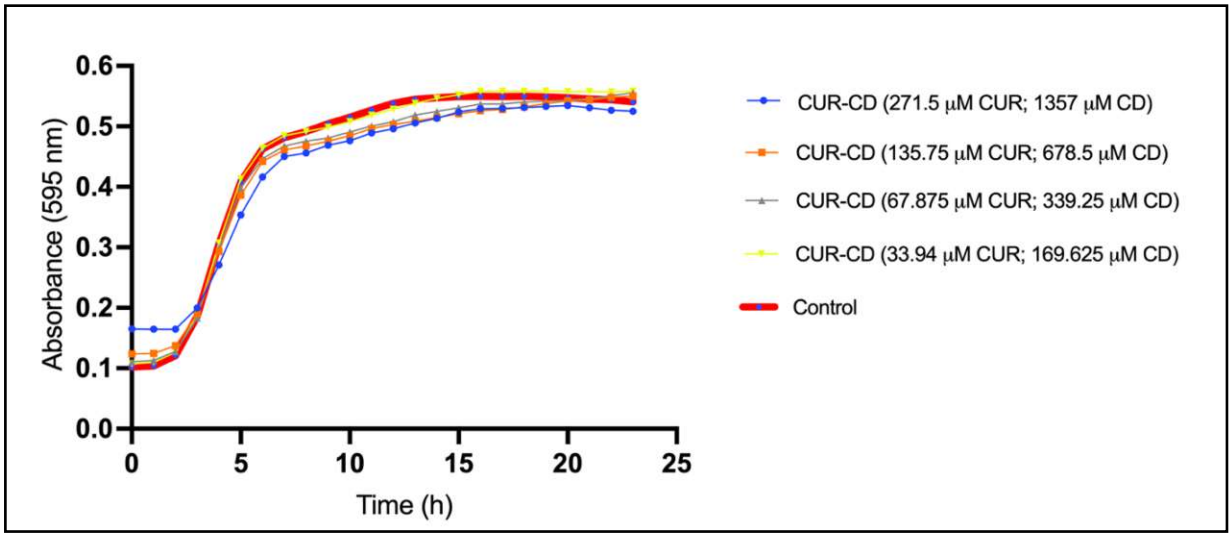

Figure 23. Bacterial growth in TSB broth, incubated for 24 h at 37 °C, after applying CUR-CD complex at different concentrations

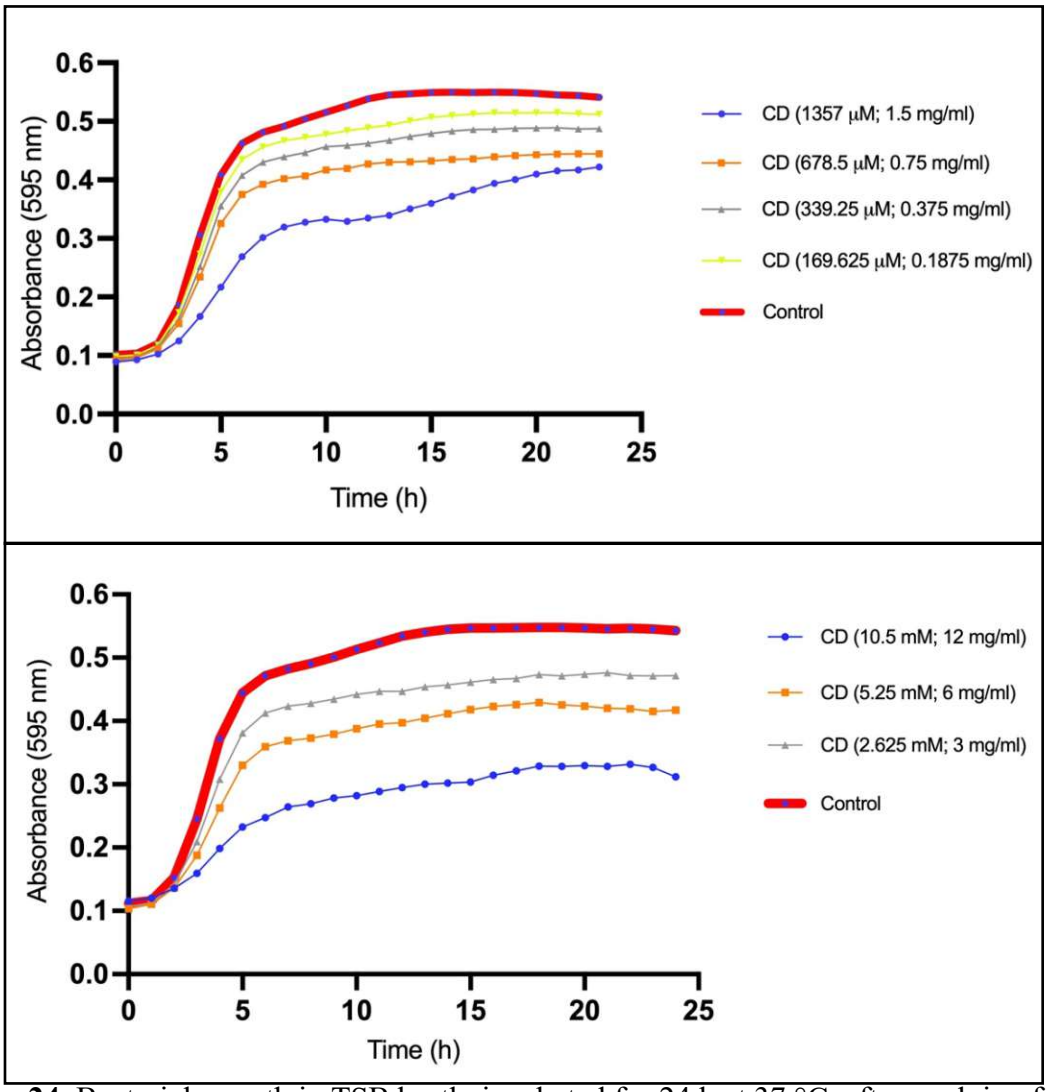

Figure 24. Bacterial growth in TSB broth, incubated for 24 h at 37 °C, after applying free β-cyclodextrin at different concentrations

CONCLUSIONS AND OUTLOOK

This study aimed to determine the potential of using β-cyclodextrins (β-CDs) and CD-decorated SPIONs (CySPIONs) in improving the delivery of curcumin (CUR) and using the harvesting effect of CD for extraction of cholesterol and reducing bacterial growth. We demonstrated the feasibility of β-CD to encapsulate CUR via inclusion complexation using the solvent evaporation method. Our study shows that CUR was efficiently encapsulated into the cavity of β-CD and the formation of the inclusion complex was confirmed using IR and UV-Vis spectroscopy, DSC, and DLS.

We investigated the cholesterol-mopping activity of free β-CDs, CySPIONs, CUR-CD, and CUR-CySPION in cholesterol-impaired CHO cell lines. The ability of free β-CDs and CySPIONs to sequester cholesterol is concentration-dependent – the higher their concentration, the more cholesterol is solubilized. When loaded with curcumin, CUR-CySPION achieved better cholesterol-mopping activity than CUR-CD, suggesting a better uptake of CUR-CySPION. Similarly, a higher amount of solubilized cholesterol was achieved for empty CySPIONs than for empty free CDs. A possible improvement of this study would be applying a chemical modification of β-CD, e.g., 2-hydroxypropyl-β-cyclodextrin (HPβCD), which is already in clinical trials for its proven ability to lower whole-body cholesterol content. Understanding and optimizing how the CDs relieve cholesterol accumulation in NPC mutant cells will contribute to the development of effective therapeutic approaches for neurodegenerative lipid storage disorders such as NPC.

In vitro studies suggest that curcumin inhibits cancer cell growth by activating apoptosis, but the mechanism underlying these effects is still unclear. Here, we investigated the apoptotic properties of CUR, CUR-CD, and CUR-CySPION-treated HepG2 cells. We assessed the ability of curcumin delivered either CD or CySPIONs to induce apoptosis in HepG2 cells. We found that free CUR was time-dependent in triggering apoptosis, being the most effective in the first 24h. When delivering curcumin in an inclusion complex either as CUR-CD or CUR-CySPIONs, curcumin appeared to be less effective in the same time range in promoting apoptosis. Curcumin complexed inside the CD cavity is not active and must be released. The rate of release is determined by the affinity of the CUR-CD complex and will delay the onset of apoptosis until sufficient amounts of curcumin have been released. The cell viability assay of HepG2 cells showed free CUR at 60 μM to be highly toxic for cells after 48 h while CUR-CD and CUR-CySPION appeared to be less toxic in the same time frame. In the future, we should explore a wider range of concentrations of applied curcumin and follow their

efficacy over a longer time scale. Additionally, a necrosis assay would give information about the curcumin concentrations inducing apoptosis or necrosis.

Finally, free CUR, β-CD, and curcumin-loaded cyclodextrins were tested in *Staphylococcus aureus* to determine MIC and MBC. Neither CUR nor CUR-CD showed bacterial inhibition, although CUR delayed bacterial growth at high concentrations. Surprisingly, free β-CD showed more antibacterial activity than CUR and CUR-CD, although when seeding them on an agar plates, they did not possess a direct bactericidal effect against *S. aureus* at the same concentrations. Research has demonstrated that cyclodextrins might influence quorum sensing driven processes. However, their effects on bacterial communication regulated processes are still poorly known. In the future, we should test the time-, temperature-, and concentration-dependent efficacy of various cyclodextrins and their derivatives, even applying a combination of cyclodextrins.

The results of this study show the necessity of investing in the improvement of the biological activity of both curcumin and cyclodextrins, and in research regarding the investigation of the biotechnological potential of these substances, especially their antibacterial effects and their modulatory effect on cell growth through apoptosis and necrosis.

ACKNOWLEDGEMENTS

First and foremost, I am indebted to Prof. Erik Reimhult for believing in this project and making it possible to do my master's thesis in your group at the Department of Nanobiotechnology (DNBT) of the University of Natural Resources and Life Sciences (BOKU) in Vienna.

I am grateful to my supervisor, Dr. Antonino Puglisi. Without his assistance and dedicated involvement in every step throughout the research, this thesis would have never been accomplished. I would like to thank you very much for your support and understanding over these past few months. Your insightful feedback pushed me to sharpen my thinking and brought my work to a higher level.

I would also like to thank the experts who were involved in this research project. Without their passionate participation and input, this paper could not have been successfully conducted. Many thanks to Andrea Scheberl for her steadfast help with the cell cultures, viability tests, and to Dr. Guruprakash Subbiahdoss for his help and expertise, and for making the antibacterial experiments possible.

I would also like to acknowledge Dr. Peter Ertl at the Vienna University of Technology as the second reader of this thesis. I am gratefully obliged for his very valuable comments on this thesis and for guiding me in the last steps towards the diploma.

Finally, I must express my very profound gratitude to my parents and my partner and friends for providing me with unfailing support and continuous encouragement throughout my years of study and through the process of researching and drafting this thesis. This accomplishment would not have been possible without them. These have been the most challenging times of my life. I had many mountains to climb, thank you for helping me through the many hurdles.

REFERENCES

[1] R. P. Feynman, “There’s plenty of room at the bottom,” *California Institute of Technology Journal of Engineering and Science*. pp. 4(2), 23–36, 1960.

[2] I. Khan, K. Saeed, and I. Khan, “Nanoparticles: Properties, applications and toxicities,” *Arab. J. Chem.*, vol. 12, no. 7, pp. 908–931, 2019.

[3] P. Walter *et al.*, “Early use of PbS nanotechnology for an ancient hair dyeing formula,” *Nano Lett.*, vol. 6, no. 10, pp. 2215–2219, 2006.

[4] G. Chiari, R. Giustetto, J. Druzik, E. Doehne, and G. Ricchiardi, “Pre-columbian nanotechnology: Reconciling the mysteries of the maya blue pigment,” *Appl. Phys. A Mater. Sci. Process.*, vol. 90, no. 1, pp. 3–7, 2008.

[5] S. C. Alter and B. H. Hakonsson, “On Slaves and Silk Hankies Seeking Truth in Damascus Steel,” 2017.

[6] T. H. E. Cup, D. The, D. Of, V. Temper, and O. N. E. O. F. His, “The Lycurgus Cup - A Roman Nanotechnology.”

[7] D. A. Taylor, “Dust in the wind,” *Environ. Heal.*, vol. 110, no. 2, pp. 80–87.

[8] L. C. Fuller, “Podoconiosis: Endemic nonfilarial elephantiasis,” *Curr. Opin. Infect. Dis.*, vol. 18, no. 2, pp. 119–122, 2005.

[9] J. Waye, “Classic Kaposi ’ s southern Italy,” 1995.

[10] J. Jeevanandam, A. Barhoum, Y. S. Chan, A. Dufresne, and M. K. Danquah, “Review on nanoparticles and nanostructured materials: History, sources, toxicity and regulations,” *Beilstein J. Nanotechnol.*, vol. 9, no. 1, pp. 1050–1074, 2018.

[11] D. A. Bazylinski, A. J. Garratt-Reed, and R. B. Frankel, “Electron microscopic studies of magnetosomes in magnetotactic bacteria,” *Microsc. Res. Tech.*, vol. 27, no. 5, pp. 389–401, 1994.

[12] A. Arakaki, H. Nakazawa, M. Nemoto, T. Mori, and T. Matsunaga, “Formation of magnetite by bacteria and its application,” *J. R. Soc. Interface*, vol. 5, no. 26, pp. 977–999, 2008.

[13] N. A. Patankar, “Mimicking the lotus effect: Influence of double roughness structures and slender pillars,” *Langmuir*, vol. 20, no. 19, pp. 8209–8213, 2004.

[14] K. Autumn and N. Gravish, “Gecko adhesion: evolutionary nanotechnology,” *Philos. Trans. R. Soc. A Math. Phys. Eng. Sci.*, vol. 366, no. 1870, pp. 1575–1590, 2008.

[15] W. P. Linak, C. A. Miller, and J. O. L. Wendt, “Comparison of particle size distributions and elemental partitioning from the combustion of pulverized coal and residual fuel oil,” *J. Air Waste Manag. Assoc.*, vol. 50, no. 8, pp. 1532–1544, 2000.

[16] K. E. Kelly, D. Wagner, J. A. S. Lighty, and A. F. Sarofim, “Real-time measurements of jet aircraft engine exhaust,” *J. Air Waste Manag. Assoc.*, vol. 55, no. 5, pp. 583–

593, 2005.

[17] K. F. Soto, A. Carrasco, T. G. Powell, K. M. Garza, and L. E. Murr, “Comparative in vitro cytotoxicity assessment of some manufactured nanoparticulate materials characterized by transmissionelectron microscopy,” *J. Nanoparticle Res.*, vol. 7, no. 2–3, pp. 145–169, 2005.

[18] Z. Ning, C. S. Cheung, J. Fu, M. A. Liu, and M. A. Schnell, “Experimental study of environmental tobacco smoke particles under actual indoor environment,” *Sci. Total Environ.*, vol. 367, no. 2–3, pp. 822–830, 2006.

[19] L. Rushton, “Health impact of environmental tobacco smoke in the home,” *Rev. Environ. Health*, vol. 19, no. 3–4, pp. 291–309, 2004.

[20] D. Stefani, D. Wardman, and T. Lambert, “The implosion of the calgary general hospital: Ambient air quality issues,” *J. Air Waste Manag. Assoc.*, vol. 55, no. 1, pp. 52–59, 2005.

[21] M. F. L. De Volder, S. H. Tawfick, R. H. Baughman, and A. J. Hart, “Carbon nanotubes: Present and future commercial applications,” *Science (80-.).*, vol. 339, no. 6119, pp. 535–539, 2013.

[22] A. Weir, P. Westerhoff, L. Fabricius, K. Hristovski, and N. Von Goetz, “Titanium dioxide nanoparticles in food and personal care products,” *Environ. Sci. Technol.*, vol. 46, no. 4, pp. 2242–2250, 2012.

[23] M. Sadat-Shojai, M. Atai, A. Nodehi, and L. N. Khanlar, “Hydroxyapatite nanorods as novel fillers for improving the properties of dental adhesives: Synthesis and application,” *Dent. Mater.*, vol. 26, no. 5, pp. 471–482, 2010.

[24] M. Cao, J. Li, J. Tang, C. Chen, and Y. Zhao, “Gold Nanomaterials in Consumer Cosmetics Nanoproducts: Analyses, Characterization, and Dermal Safety Assessment,” *Small*, vol. 12, no. 39, pp. 5488–5496, 2016.

[25] R. Rampado, S. Crotti, P. Caliceti, S. Pucciarelli, and M. Agostini, “Recent Advances in Understanding the Protein Corona of Nanoparticles and in the Formulation of ‘Stealthy’ Nanomaterials,” *Front. Bioeng. Biotechnol.*, vol. 8, no. April, pp. 1–19, 2020.

[26] S. J. Park, “Protein–nanoparticle interaction: Corona formation and conformational changes in proteins on nanoparticles,” *Int. J. Nanomedicine*, vol. 15, pp. 5783–5802, 2020.

[27] M. Hadjidemetriou and K. Kostarelos, “Nanomedicine: Evolution of the nanoparticle corona,” *Nat. Nanotechnol.*, vol. 12, no. 4, pp. 288–290, 2017.

[28] I. L. and K. A. Dawson, “Protein-nanoparticle interactions,” *Nano Today*, vol. 3, no. 1, pp. 40–47, 2008.

[29] G. Settanni *et al.*, “Protein corona composition of poly(ethylene glycol)-and poly (phosphoester)-coated nanoparticles correlates strongly with the amino acid composition of the protein surface,” *Nanoscale*, vol. 9, no. 6, pp. 2138–2144, 2017.

[30] A. Mukhopadhyay, S. Basu, S. Singha, and H. K. Patra, “Inner-view of nanomaterial incited protein conformational changes: Insights into designable interaction,” *Research*, vol. 2018, 2018.

[31] M. H. Ja’Far *et al.*, “Inclusion of curcumin in β-cyclodextrins as potential drug delivery system: Preparation, characterization and its preliminary cytotoxicity approaches,” *Sains Malaysiana*, vol. 47, no. 5, pp. 977–989, 2018.

[32] S. Fu and R. Kurzrock, “Development of curcumin as an epigenetic agent,” *Cancer*, vol. 116, no. 20, pp. 4670–4676, 2010.

[33] M. H. Teiten, S. Eifes, M. Dicato, and M. Diederich, *Curcumin-the paradigm of a multi-target natural compound with applications in cancer prevention and treatment*, vol. 2, no. 1. 2010.

[34] E. Shankar, R. Kanwal, M. Candamo, and S. Gupta, “Dietary phytochemicals as epigenetic modifiers in cancer: Promise and challenges,” *Semin. Cancer Biol.*, vol. 40_41, pp. 82–99, 2016.

[35] L. Neckers *et al.*, “Curcumin is an Inhibitor of p300 Histone Acetylatransferase,” *Med. Chem. (Los. Angeles).*, vol. 2, no. 2, pp. 169–174, 2006.

[36] A. Rodriguez-Garcia *et al.*, “Thioredoxin 1 modulates apoptosis induced by bioactive compounds in prostate cancer cells,” *Redox Biol.*, vol. 12, pp. 634–647, 2017.

[37] C. S. Mangolim *et al.*, “Curcumin-β-cyclodextrin inclusion complex: Stability, solubility, characterisation by FT-IR, FT-Raman, X-ray diffraction and photoacoustic spectroscopy, and food application,” *Food Chem.*, vol. 153, pp. 361–370, 2014.

[38] D. Dhivya and A. N. Rajalakshmi, “Curcumin Nano Drug Delivery Systems: A Review on its Type and Therapeutic Application,” *Pharmatutor*, vol. 5, no. 12, p. 30, 2017.

[39] J. K. Trigo-gutierrez, Y. Vega-chacón, A. B. Soares, and E. G. de O. Mima, *Antimicrobial activity of curcumin in nanoformulations: A comprehensive review*, vol. 22, no. 13. 2021.

[40] M. E. Davis and M. E. Brewster, “Cyclodextrin-based pharmaceutics: Past, present and future,” *Nat. Rev. Drug Discov.*, vol. 3, no. 12, pp. 1023–1035, 2004.

[41] C. Coisne, S. Tilloy, E. Monflier, D. Wils, L. Fenart, and F. Gosselet, “Cyclodextrins as emerging therapeutic tools in the treatment of cholesterol-associated vascular and neurodegenerative diseases,” *Molecules*, vol. 21, no. 12, pp. 1–22, 2016.

[42] P. Buchwald and N. Bodor, “Brain-Targeting Chemical Delivery Systems and Their Cyclodextrin-Based Formulations in Light of the Contributions of Marcus E. Brewster,” *J. Pharm. Sci.*, vol. 105, no. 9, pp. 2589–2600, 2016.

[43] M. S. Brown and J. L. Goldstein, “A proteolytic pathway that controls the cholesterol content of membranes, cells, and blood,” *Proc. Natl. Acad. Sci. U. S. A.*, vol. 96, no. 20, pp. 11041–11048, 1999.

[44] F. W. Pfrieger, “Cholesterol homeostasis and function in neurons of the central nervous system,” *Cell. Mol. Life Sci.*, vol. 60, no. 6, pp. 1158–1171, 2003.

[45] M. Mondal, B. Mesmin, S. Mukherjee, and F. R. Maxfield, “Sterols Are Mainly in the Cytoplasmic Leaflet of the Plasma Membrane and the Endocytic Recycling Compartment in CHO Cells,” *Mol. Biol. Cell*, vol. 20, pp. 581–588, 2009.

[46] T. Suzuki, “Lipid rafts at postsynaptic sites: Distribution, function and linkage to postsynaptic density,” *Neurosci. Res.*, vol. 44, no. 1, pp. 1–9, 2002.

[47] F. D. Porter and G. E. Herman, “Malformation syndromes caused by disorders of cholesterol synthesis,” *J. Lipid Res.*, vol. 52, no. 1, pp. 6–34, 2011.

[48] M. T. Vanier, “Niemann-Pick disease type C Disease definition,” *Vanier Orphanet J. Rare Dis.*, vol. 5, pp. 1–18, 2010.

[49] C. M. Ramirez *et al.*, “Weekly cyclodextrin administration normalizes cholesterol metabolism in nearly every organ of the niemann-pick type C1 mouse and markedly prolongs life,” *Pediatr. Res.*, vol. 68, no. 4, pp. 309–315, 2010.

[50] L. Szente, A. Singhal, A. Domokos, and B. Song, “Cyclodextrins: Assessing the impact of cavity size, occupancy, and substitutions on cytotoxicity and cholesterol homeostasis,” *Molecules*, vol. 23, no. 5, pp. 1–15, 2018.

[51] A. Puglisi and Y. Yagci, “Cyclodextrin-Based Macromolecular Systems as Cholesterol-Mopping Therapeutic Agents in Niemann–Pick Disease Type C,” *Macromol. Rapid Commun.*, vol. 40, no. 1, pp. 1–6, 2019.

[52] A. Lassenberger, O. Bixner, T. Gruenewald, H. Lichtenegger, R. Zirbs, and E. Reimhult, “Evaluation of High-Yield Purification Methods on Monodisperse PEG-Grafted Iron Oxide Nanoparticles,” *Langmuir*, vol. 32, no. 17, pp. 4259–4269, 2016.

[53] H. Mok and M. Zhang, “Superparamagnetic iron oxide nanoparticle-based delivery systems for biotherapeutics,” *Expert Opin. Drug Deliv.*, vol. 10, no. 1, pp. 73–87, 2013.

[54] A. Puglisi, S. Bassini, and E. Reimhult, “Cyclodextrin-Appended Superparamagnetic Iron Oxide Nanoparticles as Cholesterol-Mopping Agents,” *Front. Chem.*, vol. 9, no. November, pp. 1–8, 2021.

[55] S. Rahman, S. Cao, K. J. Steadman, M. Wei, and H. S. Parekh, “Native and ß-cyclodextrin-enclosed curcumin: Entrapment within liposomes and their in vitro cytotoxicity in lung and colon cancer,” *Drug Deliv.*, vol. 19, no. 7, pp. 346–353, 2012.

[56] M. L. C. Passos, M. C. Sarraguça, and M. L. M. F. S. Saraiva, “Spectrophotometry | organic compounds,” *Encycl. Anal. Sci.*, vol. 9, no. July 2018, pp. 236–243, 2019.

[57] L. G. P. Moraes, R. S. F. Rocha, L. M. Menegazzo, E. B. De Araújo, K. Yukimitu, and J. C. S. Moraes, “Infrared spectroscopy: A tool for determination of the degree of conversion in dental composites,” *J. Appl. Oral Sci.*, vol. 16, no. 2, pp. 145–149, 2008.

[58] W. F. Haines PJ, Reading, M, *Differential thermal analysis and differential scanning*

calorimetry. In Brown ME (ed): Handbook of Thermal Analysis and Calorimetry, vol 1. The Netherlands: Elsevier Science BV, 1998;16-21. .

[59] D. RL, "New heat flux DSC measurement technique. Ther- mochim Acta 2002;395:201–208." .

[60] Malvern and M. Instruments, "Dynamic Light Scattering : An Introduction in 30 Minutes," *Tech. Note MRK656-01*, pp. 1–8, 2011.

[61] J. Stetefeld, S. A. McKenna, and T. R. Patel, "Dynamic light scattering: a practical guide and applications in biomedical sciences," *Biophys. Rev.*, vol. 8, no. 4, pp. 409–427, 2016.

[62] N. P. Pennycook SJ, *Scanning Transmission Electron Microscopy*. New York, NY: Springer New York, 2011.

[63] F. M. Wurm, "Production of recombinant protein therapeutics in cultivated mammalian cells," *Nat. Biotechnol.*, vol. 22, no. 11, pp. 1393–1398, 2004.

[64] J. O'Brien, I. Wilson, T. Orton, and F. Pognan, "Investigation of the Alamar Blue (resazurin) fluorescent dye for the assessment of mammalian cell cytotoxicity," *Eur. J. Biochem.*, vol. 267, no. 17, pp. 5421–5426, 2000.

[65] M. J. G.-L. María Teresa Donato, Laia Tolosa, "Culture and Functional Characterization of Human Hepatoma HepG2 Cells," *Methods Mol Biol.*, vol. 1250, pp. 77–93, 2015.

[66] A. A. T. Bioquest, "Caspase 3/7 Activity Apoptosis Assay Kit * Red Fluorescence *," no. November, pp. 2–3, 2019.

[67] S. Y. C. Tong, J. S. Davis, E. Eichenberger, T. L. Holland, and V. G. Fowler, "Staphylococcus aureus infections: Epidemiology, pathophysiology, clinical manifestations, and management," *Clin. Microbiol. Rev.*, vol. 28, no. 3, pp. 603–661, 2015.

[68] F. R. DeLeo, B. A. Diep, and M. Otto, "Host Defense and Pathogenesis in Staphylococcus aureus Infections," *Infect. Dis. Clin. North Am.*, vol. 23, no. 1, pp. 17–34, 2009.

[69] K. Y. Le and M. Otto, "Quorum-sensing regulation in staphylococci-an overview," *Front. Microbiol.*, vol. 6, no. OCT, pp. 1–8, 2015.

[70] P. Parvekar, J. Palaskar, S. Metgud, R. Maria, and S. Dutta, "The minimum inhibitory concentration (MIC) and minimum bactericidal concentration (MBC) of silver nanoparticles against Staphylococcus aureus," *Biomater. Investig. Dent.*, vol. 7, no. 1, pp. 105–109, 2020.

[71] J. Chen, X. Qin, S. Zhong, S. Chen, W. Su, and Y. Liu, "Characterization of curcumin/cyclodextrin polymer inclusion complex and investigation on its antioxidant and antiproliferative activities," *Molecules*, vol. 23, no. 5, 2018.

[72] F. Trotta, M. Zanetti, and G. Camino, "Thermal degradation of cyclodextrins," *Polym.*

Degrad. Stab., vol. 69, no. 3, pp. 373–379, 2000.

[73] M. H. Ucisik, S. Küpcü, B. Schuster, and U. B. Sleytr, "Characterization of CurcuEmulsomes: Nanoformulation for enhanced solubility and delivery of curcumin," *J. Nanobiotechnology*, vol. 11, no. 1, pp. 1–13, 2013.

[74] A. Moustapha *et al.*, "Curcumin induces crosstalk between autophagy and apoptosis mediated by calcium release from the endoplasmic reticulum, lysosomal destabilization and mitochondrial events," *Cell Death Discov.*, vol. 1, no. 1, 2015.

[75] Z. Berkl *et al.*, "Effect of Cyclodextrins on the Biofilm Formation Capacity of Pseudomonas aeruginosa PAO1," *Molecules*, vol. 27, no. 11, p. 3603, 2022.